nature communications

Article

https://doi.org/10.1038/s41467-025-66212-x

Endothelial RAB5IF is required for pathological and developmental retinal angiogenesis

Received: 17 January 2025

Accepted: 3 November 2025

Published online: 13 December 2025

Check for updates

Wen Bai[1,6], De-pei Yin[2,6], Gang Chen[3,6], Yao Lu[1,6], Qin Jiang[1], Ke-ran Li[1,7] ✉, Jin Yao[1,7] ✉ & Cong Cao[4,5,7] ✉

Retinal angiogenesis drives both normal vascular development and sight-threatening retinal vascular diseases. While mitochondria are known to fuel this process, the roles of many specific mitochondrial proteins are poorly understood. Here we show that the mitochondrial protein RAB5 interacting factor (RAB5IF) as a critical pro-angiogenic regulator of physiological retinal vascular development in neonatal mice (sex-balanced) and pathological retinal angiogenesis in two models: oxygen-induced retinopathy mice (sex-balanced) and laser-induced choroidal neovascularization mice (sex-balanced). Proteomic sequencing identified SUMO2 as a critical downstream protein of RAB5IF. RAB5IF silencing impeded mitochondrial respiration and ribosome biogenesis, specifically suppressing *SUMO2* mRNA translation initiation and consequently lowering SUMO2 protein levels in retinal microvascular endothelial cells. We also identify that SUMO2-mediated SUMOylation of Gαi1/3 is required for their roles in mediating VEGF signaling. Mutations at the SUMOylation sites of Gαi1/3 hindered VEGF-induced signaling and pro-angiogenic activity. Together, these findings delineate a RAB5IF-SUMO2-Gαi1/3 signaling axis essential for retinal angiogenesis, presenting new therapeutic targets for neovascular eye diseases.

Abnormal angiogenesis is a hallmark of several common retinal and ocular diseases, including age-related macular degeneration (AMD), diabetic retinopathy (DR), and retinal vein occlusion[1–3]. It is characterized by excessive and aberrant formation of blood vessels, leading to significant disruptions in retinal architecture and function[1–3]. In AMD, choroidal neovascularization (CNV) results in the infiltration of abnormal blood vessels beneath the retinal pigment epithelium (RPE), causing retinal detachment and subsequent photoreceptor degeneration[4]. In DR, chronic hyperglycemia induces a cascade of biochemical changes that promote retinal ischemia and neovascularization, leading to further complications such as vitreous hemorrhage and tractional retinal detachment[5]. Key factors driving this process include vascular endothelial growth factor (VEGF), fibroblast growth factor (FGF), and pro-inflammatory factors, influenced by hypoxic conditions and/or inflammation[1].

Activated endothelial cells, instrumental in angiogenesis, secrete an array of matrix metalloproteinases (MMPs) that degrade the basement membrane, enabling cellular invasion[6–8]. Upon angiogenic stimuli, endothelial tip cells exhibit directional migration, extending filopodia and lamellipodia to guide sprout growth. As leading-edge sensors, tip cells direct vascular development, while stalk cells predominantly proliferate for sprout elongation and lumen formation[6–8].

[1]The Affiliated Eye Hospital, Nanjing Medical University, Nanjing, China. [2]Department of Otorhinolaryngology Head and Neck Surgery, The Children's Hospital Affiliated to Soochow University, Suzhou, China. [3]Department of Neurosurgery, the First Affiliated Hospital of Soochow University, Suzhou, Jiangsu, China. [4]Institution of Neuroscience, Soochow University, Suzhou, China. [5]Department of Orthopedics, Affiliated Hospital of Youjiang Medical University for Nationalities, Guangxi Key Laboratory of basic and translational research of Bone and Joint Degenerative Diseases, Guangxi Biomedical Materials Engineering Research Center for Bone and Joint Degenerative Diseases, Baise, China. [6]These authors contributed equally: Wen Bai, De-pei Yin, Gang Chen, Yao Lu. [7]These authors jointly supervised this work: Ke-ran Li, Jin Yao, and Cong Cao. ✉e-mail: likeran@njmu.edu.cn; dryaojin@126.com; caocong@suda.edu.cn

Tip cell convergence coalesces sprouts into perfused vessels, signaling the transition from angiogenesis to vascular maturation[6–9]. This perfusion recruits pericytes and reforms the basement membrane, stabilizing new blood vessels[6–9]. These interactions demonstrate the dynamic regulation of angiogenesis

Mitochondria, pivotal regulators of cellular metabolism, energy production, and signaling, play a crucial role in endothelial cell function and angiogenesis[10–12]. They provide ATP for the energy-demanding processes of endothelial cell proliferation and migration[10–12]. Beyond ATP synthesis, mitochondria generate reactive oxygen species (ROS), which act as signaling molecules modulating angiogenic responses[10–12]. The angiogenic shift towards aerobic glycolysis supports the biosynthetic demands of capillary formation and maintenance[10–12]. Mitochondrial morphology dynamics, involving fission and fusion, are also important for endothelial cell integrity and function, facilitating the distribution of mitochondrial content during cell proliferation and migration[10–12]. Moreover, mitochondria interact with the cytoskeleton to influence cell shape and motility, crucial for vascular network formation[10–12].

RAB5IF (RAB5 interacting factor) is a mitochondrial protein that has attracted significant attention in recent research[13]; however, its specific functions and roles within mitochondrial biology remain largely unexplored and inadequately characterized. A recent study employed CRISPR-mediated knockout cells together with mass spectrometry-based multiomics analyses have identified RAB5IF as an important mitochondrial protein associated with pathogenic variants linked to cerebrofaciothoracic dysplasia[13]. These results show that RAB5IF may play a significant role in mitochondrial function. However, the specific mechanisms underlying its function remain to be elucidated[13]. Ma *et al.* have shown that *RAB5IF* is upregulated in SONFH (steroid-induced osteonecrosis of the femoral head) tissues[14]. Chen et al. demonstrated that *RAB5IF* is upregulated in hepatocellular carcinoma. Furthermore, in conjunction with other genetic markers, *RAB5IF* may serve as a potential predictor of patient survival and clinical risk[15]. However, the expression, functional role, and underlying mechanisms of RAB5IF in endothelial cells and angiogenesis are uncharacterized. In this study, we demonstrate that endothelial RAB5IF is essential for both physiological and pathological retinal angiogenesis.

G protein subunit alpha i (Gαi) proteins consist of three isoforms: Gαi1, Gαi2, and Gαi3. These Gαi proteins are known to interact with G protein-coupled receptors (GPCRs) to inhibit the activation of adenylyl cyclase, leading to a reduction in cyclic AMP (cAMP) levels[16,17]. Our research highlights the critical roles of Gαi1 and Gαi3 in angiogenesis[18–22], as they facilitate VEGF-induced endocytosis of VEGFR2, activating the Akt-mTOR and Erk-MAPK pathways in endothelial cells[22]. Additionally, in endothelial cells, Gαi1 and Gαi3 interact with the c-Kit receptor, activated by stem cell factor (SCF), to enhance angiogenesis[19]. Gαi1 and Gαi3 also form a complex with CD146 in response to Netrin-1 in endothelial cells, further promoting angiogenesis via Akt-mTOR activation[20]. Moreover, our recent study shows that phosphoenolpyruvate carboxykinase 1 (PCK1) promotes Gαi3 expression, enhancing Akt-mTOR activation through GATA binding protein 4 (GATA4)[21]. The association of Gαi1 and Gαi3 with the RSPO3 (R-spondin 3)-activated receptor LGR4 (leucine-rich repeat G protein-coupled receptor 4) is significant for downstream Akt-mTOR activation and angiogenesis[20]. The findings of this study demonstrate that RAB5IF enhances angiogenesis, possibly through its target protein small ubiquitin-like modifier 2 (SUMO2)-mediated SUMOylation of Gαi1 and Gαi3 in endothelial cells.

Results

Endothelial knockdown of RAB5IF inhibits retinal neovascularization in oxygen-induced retinopathy mice

We first examined the cellular expression and distribution of *RAB5IF* in oxygen-induced retinopathy (OIR) model characterized by pathological retinal neovascularization[23]. After removing the batch effects, dimensionality reduction, and annotating cells, we analyzed single-cell retinal data from the OIR model and age-matched controls under normoxia ("NORM") (GSE150703) (Fig. 1A and B). The UMAP (uniform manifold approximation and projection) plot demonstrated that *RAB5IF* is expressed across various retinal cell types (Fig. 1A–C). Differential analysis revealed upregulation of *RAB5IF* transcripts in endothelial cells (ECs) and pericytes of the retinas of OIR mice (Fig. 1D), and it was downregulated in amacrine, cone, and rod cells (Fig. 1D). Volcano plot indicated a significant increase in *RAB5IF* transcripts in retinal endothelial cells of OIR mice compared to the age-matched controls (Fig. 1E).

qRT-PCR and Western blotting assays of the primary murine retinal microvascular endothelial cells (mRMECs) isolated from P17 normoxia and P17 OIR mice revealed significantly elevated *RAB5IF* mRNA and protein levels in the OIR model (Fig. 1F), aligning with single-cell sequencing findings. Immunofluorescence staining of P17 OIR retinal flat mounts revealed RAB5IF (green) predominantly within neovascular tufts extending into the vitreous, localizing to both IB4-stained endothelial cells and NG2-stained pericytes (Fig. 1G). We also sub-clustered the retinal endothelial cell population derived from the OIR single-cell dataset into tip, proliferating, and resting cells (Fig. 1H). UMAP and dot plots indicated that *RAB5IF* is mainly distributed in proliferating endothelial cells of P17 OIR mice (Fig. 1H).

To investigate the effect of RAB5IF on pathological retinal neovascularization, we administered AAV encoding two different AAV^{ENT}-ICAM2p-shRAB5IFs via retro-orbital injection to P3 mice for endothelial-specific knockdown of RAB5IF (RAB5IF-eKD#1/RAB5IF-eKD#2, representing two different shRNA sequences). Control groups received the same AAV vector but carrying a scrambled control shRNA (shC). To verify the construct, AAV^{ENT}-ICAM2p-GFP control construct was injected, and GFP signaling localized specifically within the retinal vasculature (IB4 staining) at P17 OIR mice (Fig. S1B). The qRT-PCR and Western blotting analyses of mRMECs at P17 OIR mice confirmed successful knockdown of RAB5IF by RAB5IF-eKD#1 and RAB5IF-eKD#2 (Fig. 1I). In retinal sections of OIR mice, RAB5IF fluorescence was significantly reduced in the vascular areas (IB4 staining) of the RAB5IF-eKD group, compared to the shC control (Fig. S1C). Visualization of the retinal vasculature using IB4 staining on day P17 indicated that RAB5IF-eKD significantly inhibited the formation of pathological de novo vessels in P17 OIR model (Fig. 1J), without impacting the size of the non-perfused area (Fig. 1J). Western blot analysis of P17 OIR retinal lysates demonstrated significantly higher protein expression of RAB5IF specifically within the tufts area (pathological neovascularization) compared to the avascular area (Fig. S1A). ELISA analysis showed that RAB5IF-eKD did not alter the levels of VEGFA in the vitreous of P17 OIR mice (Fig. 1K). These results showed that upregulation of RAB5IF in endothelial cells is important for retinal neovascularization in OIR mice.

Endothelial RAB5IF knockdown inhibits laser-induced choroidal neovascularization in mice

We further examined the expression and function of RAB5IF in pathological choroidal neovascularization. We analyzed choroidal single-cell data (GSE135922) from human age-related macular degeneration (AMD) and healthy controls (Fig. S1A and B). The UMAP plot indicated that *RAB5IF* is widely expressed in choroidal cells (Fig. S2A–C). Dot plots demonstrated that *RAB5IF* expression was significantly elevated in vascular endothelial cells of the choroid in patients with dry AMD (dAMD) and neovascular AMD (nAMD) (Fig. S2D), with higher levels observed in nAMD (Fig. S2D). To model nAMD, we constructed a laser-induced choroidal neovascularization (CNV) mouse model. RNA was extracted from primary choroidal vascular endothelial cells of age-matched controls and CNV mice. qRT-PCR assay results showed a significant increase

https://doi.org/10.1038/s41467-025-66212-x

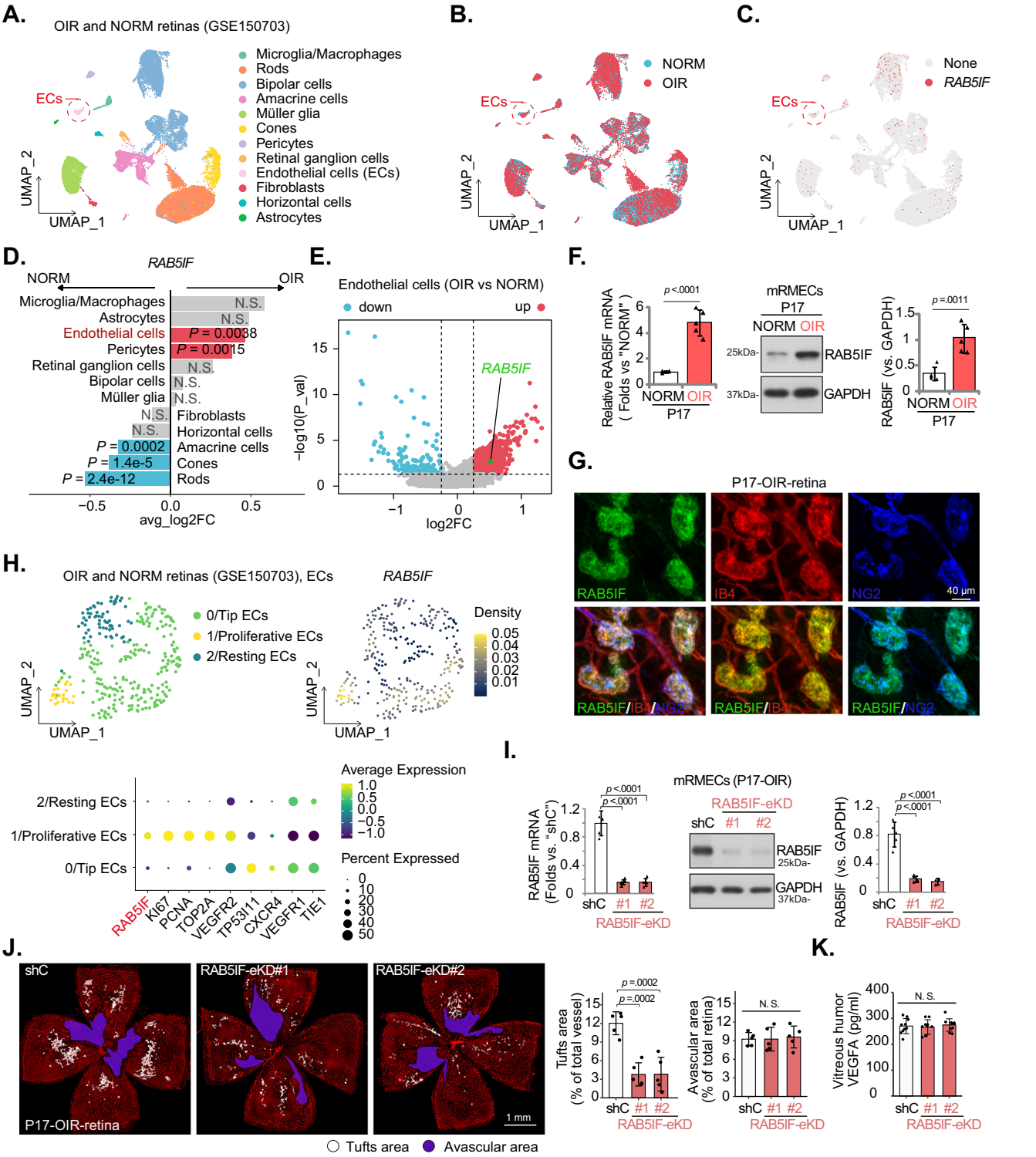

in *RAB5IF* transcript levels in choroidal vascular endothelial cells of CNV mice (Fig. S2E), aligning with bioinformatic findings from single-cell sequencing.

To investigate the effects of RAB5IF on pathological CNV, we again knocked down RAB5IF expression in choroidal endothelial cells (RAB5IF-eKD) via intravitreal injection of AAV 21 days prior to laser induction. A week post-laser induction, qRT-PCR and Western blotting of primary choroidal vascular endothelial cell suspensions confirmed successful knockdown of RAB5IF (Fig. S2F and G). Visualization of CNV dots using IB4 demonstrated that RAB5IF-eKD significantly hindered pathological neovascularization in CNV model (Fig. S2H). Ex vivo choroidal explant culture findings showed that RAB5IF-eKD resulted in a significant reduction in vascular sprout area (Fig. S2I) on day-3 and day-5. Therefore, RAB5IF-eKD significantly inhibited laser-induced choroidal neovascularization in CNV mice.

Endothelial RAB5IF knockdown hinders retinal vascular development in neonatal mice

Next, we analyzed retinal single-cell data obtained from P6 and P10 neonatal mice (GSE175895) (Fig. 2A). UMAP and dot plots show that *RAB5IF* is predominantly expressed in the vascular endothelial cells

Fig. 1 | Endothelial knockdown of RAB5IF inhibits retinal neovascularization in oxygen-induced retinopathy mice. A UMAP (uniform manifold approximation and projection) dimensionality reduction plot showing the cell annotations of GSE150703 data. **B** Group information displayed in the UMAP plot for oxygen-induced retinopathy (OIR) and age-matched normoxia mice (NORM). **C** UMAP plot illustrating the distribution of *RAB5IF* in OIR retinas. **D** Bidirectional bar graph comparing the fold changes of *RAB5IF* expression, with adjusted *P*-values shown. Blue: significant downregulation, red: significant upregulation, gray: not significant (N.S.). **E** Volcano plot highlighting differentially expressed genes (DEGs) between OIR and age-matched normal mice groups, with *RAB5IF* annotated. **F** qRT-PCR and Western blot analyses showed elevated RAB5IF levels in primary mRMECs from P17 OIR mice versus normoxia controls (pooled from 4 mice/sample, $n = 5$ samples/group, 15 μg protein/lane for WB). **G** Immunofluorescence of P17 OIR retinal flat mounts revealed RAB5IF (green) localized to pathological neovascular regions, co-stained with IB4 (red) and NG2 (blue). Scale bar = 40 μm. (Representative of three independent experiments). **H** Retinal endothelial populations from GSE150703 were subdivided by classical markers; UMAP and dot plots demonstrated *RAB5IF* expression patterns within endothelial subtypes. **I**–**K** The retro-orbital injection of endothelial-targeted AAV (1×10^{11} viral particles/7.5 μL/mouse) for RAB5IF knockdown was performed in neonatal P3 mice, followed by qRT-PCR and Western blotting analysis on P17 OIR to assess *RAB5IF* mRNA and protein levels in primary mRMECs (pooled from 4 mice/sample, $n = 5$ samples/group, 15 μg protein/lane for WB) **(I)**. IB4 staining at P17 OIR, showing representative images along with the quantification of neovascular area (white areas) and non-perfused avascular area (purple-shaded areas) in OIR mice ($n = 5$ mice per group). Scale bar = 1 mm (**J**). ELISA analysis of VEGFA levels in the vitreous in P17 OIR mice ($n = 10$ mice per group) (**K**). Data are presented as means ± S.D. "N.S." indicates no statistical difference ($P > 0.05$); Wilcoxon rank sum test with Bonferroni's post hoc test (**D**, **E**), Two-tailed Student's t-test (**F**) and one-way ANOVA with Bonferroni's post hoc test (**I**–**K**). Source data are provided as a Source Data file.

of neonatal mice (Fig. 2B and C). While a specific rod subpopulation exhibits high RAB5IF (Fig. 2B), the overall average for the whole cluster can appear lower (Fig. 2C). We further sub-clustered the vascular endothelial cell population of the P6 and P10 neonatal mouse into tip, proliferating, and resting cells (Fig. 2D–F). UMAP and dot plots results indicated that RAB5IF was primarily distributed in tip cells and proliferating cells (Fig. 2D–F). Immunofluorescence of retinal flat mounts from P6 mice showed localization of RAB5IF protein (green fluorescence) within blood vessels (Fig. 2G). Magnified images demonstrated RAB5IF expression in the tip and stalk cells at the anterior end of blood vessels (Fig. 2G), co-localizing with the tip cell marker CXCR4 (C-X-C chemokine receptor type 4) (Fig. S3A). qRT-PCR and Western blotting assays of retinal tissues from neonatal mice (P1-P7) demonstrated a gradual increase in retinal *RAB5IF* mRNA and protein levels after birth (Fig. 2H and I).

To assess the effects of RAB5IF on physiological retinal neovascularization, we specifically knocked down RAB5IF in retinal endothelial cells via retro-orbital injection of AAV at P1 mice. At P6, qRT-PCR and Western blotting of primary mRMECs verified the robust knockdown of RAB5IF (Fig. 2J and K). RAB5IF-eKD#1 and RAB5IF-eKD#2 represent two different shRNA sequences (Fig. 2J and K). Visualization of the retinal vasculature at P6 using IB4 staining demonstrated that RAB5IF-eKD significantly inhibited retinal vascular development (Fig. 2L), evidenced by marked reductions in vessel radial length, vessel density, and the number of vascular branches (Fig. 2L). Analysis at P14 revealed that RAB5IF-eKD led to a significant decrease in the vascular density across all three major retinal plexuses—superficial (SVP), intermediate (IVP), and deep (DVP)—with the intermediate vascular plexus (IVP) showing the most pronounced effect (Fig. S4A and B). These results showed that RAB5IF-eKD disrupted retinal vascular development in neonatal mice.

Additionally, we evaluated the effects of RAB5IF-eKD on retinal tip cells in P6 mice, finding significant reductions in the number of tip cells, as well as the number and length of filopodia (Fig. 2L). A significant reduction of tip cell marker proteins, CXCR4 and ESM1 (endothelial cell-specific molecule 1), was noticed in RAB5IF-eKD mRMECs, and RAB5IF protein levels decreased (Fig. 2M). The immunofluorescence staining in P6 mice retinas further confirmed a significant and dramatic reduction in the percentage of CXCR4-positive vascular area (tip cell) compared to the shC control (Fig. S3B). The EdU staining assay detected a significant reduction in the number of proliferating (EdU-positive) endothelial cells at the retinal vascular front (Fig. S4C and D). Conversely, there was a slight increase in the number of apoptotic endothelial cells in both the vascular front and posterior vessels (Fig. S4E and F). These results suggest that RAB5IF-eKD impairs retinal vascular development by disrupting the activity of tip and stalk cells at the vascular front and promoting the regression of vascular network.

Endothelial conditional knockout of RAB5IF inhibits retinal vasculature in adult mice

To further elucidate the role of RAB5IF in the retinal vasculature of adult mice, two distinct AAV5-FLEX-sgRAB5IF constructs were intravitreously injected into TIE1-Cre C57BL/6 J mice containing a ubiquitous, floxed *Cas9* allele. This intervention resulted in the generation of RAB5IF endothelial conditional knockout (RAB5IF-eCKO) mice, designated as RAB5IF-eCKO#1 and RAB5IF-eCKO#2, after a period of 21 days. Each of the two AAV5 constructs was designed to express non-overlapping sgRNA sequences targeting murine *RAB5IF*. To verify the specificity of the construct, the AAV5-FLEX-GFP viral particles were administered into the TIE1-Cre C57BL/6 J adult mice. Following the 21-day period, GFP signaling was observed to localize specifically within the retinal vasculature (IB4 staining) (Fig. 3A). Western blotting analyses conducted on primary mRMECs substantiated a marked reduction in RAB5IF protein expression in RAB5IF-eCKO#1/2 mice, when compared to that in control mice received AAV5-FLEX-sgRNA control construct (sgC) (Fig. 3B). Visualization of the retinal vascular architecture using IB4 staining indicated that RAB5IF-eCKO impeded retinal vascular branching (Fig. 3C). Furthermore, the retinal trypsin digestion assay and periodic acid-Schiff (PAS) staining demonstrated a substantial increase in the number of acellular capillaries following RAB5IF-eCKO (Fig. 3D). Results from the Evans Blue (EB) leakage assay revealed that RAB5IF-eCKO significantly increased retinal vascular leakage (Fig. 3E). The disruption of retinal vasculature is known to cause degeneration of retinal ganglion cells (RGCs). Consequently, we assessed the impact of RAB5IF-eCKO on RGCs. Double-staining of RGCs in retinal flat mounts with Tubb3 (tubulin beta 3 class III) and NeuN (neuronal nuclei), along with RBPMS (RNA-binding protein with multiple splicing) staining of RGCs in retinal sections, demonstrated that RAB5IF-eCKO led to a significant reduction in RGC numbers (Fig. 3F and G). This finding was further corroborated by a decrease in the expression of RGC marker proteins, Tubb3 and Thy-1 (thymocyte antigen 1), in the retinal tissues of RAB5IF-eCKO mice (Fig. 3H). These results together showed that RAB5IF-eCKO inhibited retinal vasculature in adult mice. Consistently, RAB5IF-eKD resulted in diminished protein expression of RGC marker proteins, Tubb3 and Thy-1, in the retinal tissues of P6 mice (Fig. 3I). We also tested RAB5IF endothelial overexpression in adult mice through retro-orbital injection of AAV (AAV^{ENT}-ICAM2p-oeRAB5IF) in eight-week-old mice (Fig. S5A). Endothelial RAB5IF overexpression (RAB5IF-eOE, Fig. S5A) did not significantly enhance retinal vascular branching, cause vascular leakage, induce acellular capillary formation, or alter RGC numbers in these healthy adult mice (Fig. S5B-E). This aligns with the known quiescent state of the mature adult retinal vasculature.

https://doi.org/10.1038/s41467-025-66212-x

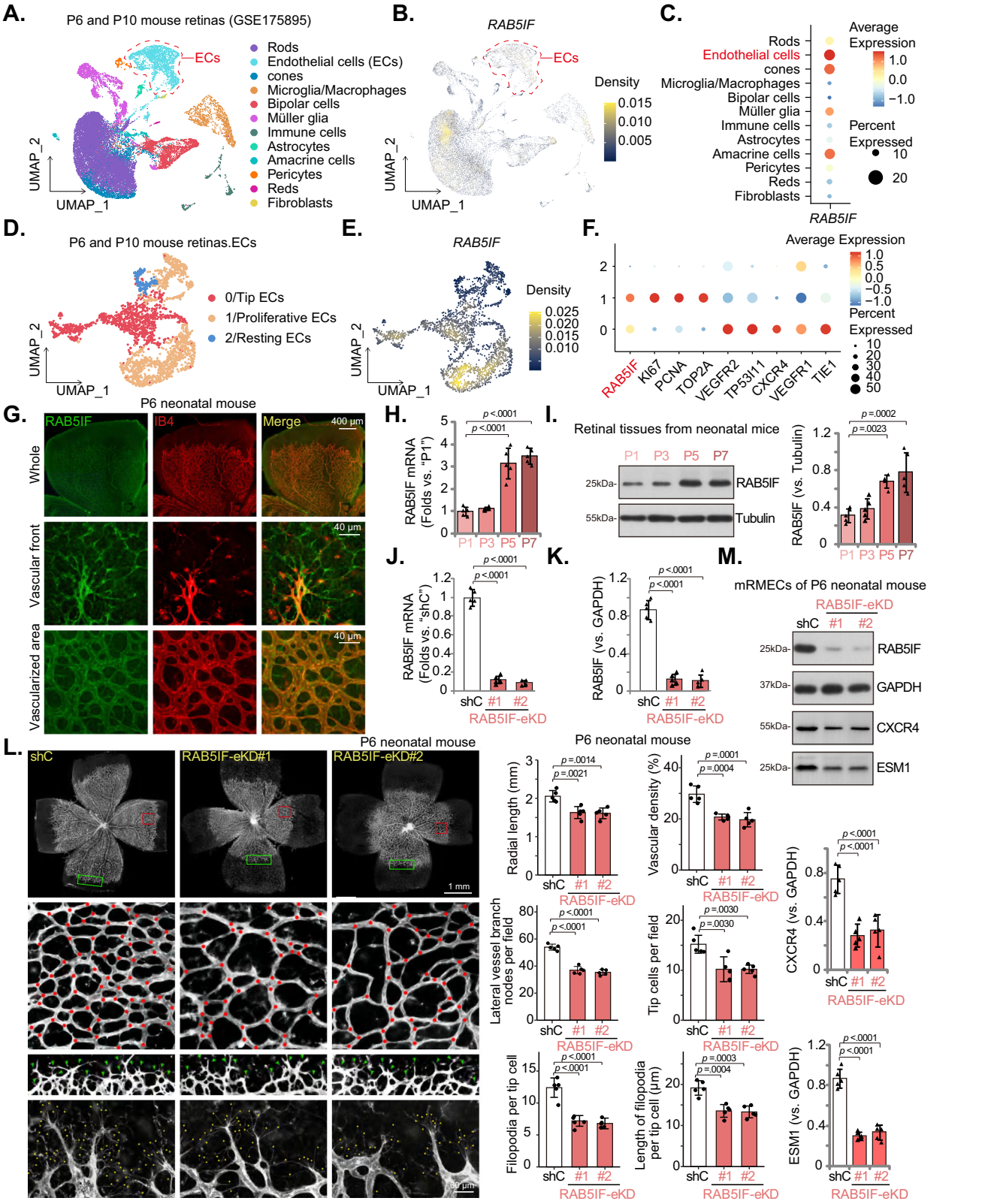

RAB5IF exerts significant pro-angiogenic activity in cultured retinal microvascular endothelial cells

To elucidate the potential role of RAB5IF in angiogenesis in vitro, human retinal microvascular endothelial cells (hRMECs) were transduced with three distinct lentiviral shRNAs targeting non-overlapping sequences of RAB5IF: shRAB5IF#1, shRAB5IF#2, and shRAB5IF#3. Following puromycin selection, stable cells were formed. Each of the three shRNAs significantly reduced both mRNA and protein levels of RAB5IF in hRMECs, when compared to it in cells treated with a scrambled control shRNA (shC) (Fig. 4A). Subsequent evaluation using an in vitro sprouting assay revealed that RAB5IF silencing markedly inhibited the sprouting of hRMECs, evidenced by a significant decrease

Fig. 2 | Endothelial RAB5IF knockdown hinders retinal vascular development in neonatal mice. A UMAP dimensionality reduction plot showing cell annotations of P6 and P10 neonatal mouse retinas (GSE175895). **B** UMAP plot illustrating the expression distribution of *RAB5IF* in P6 and P10 neonatal mouse retinas. **C** Dot plot showing the expression levels of *RAB5IF* in various retinal cell populations within P6 and P10 neonatal mouse retinas. **D**–**F** Retinal endothelial populations from GSE175895 were subdivided by classical markers; UMAP and dot plots demonstrated *RAB5IF* expression patterns within endothelial subtypes. **G** Immunofluorescence of P6 neonatal mouse retinal flat mounts, displaying RAB5IF (green fluorescence) and vasculature (IB4, red fluorescence). Scale bar = 400 μm; Magnified views of the vascular front and vascularized area were also shown. Scale bar = 40 μm. (Representative of three independent experiments). **H**, **I** qRT-PCR and Western blot analyses of RAB5IF expression across neonatal time points (individual samples, $n = 5$ mice/group, 15 μg protein/lane). **J**, **K** At P1, retro-orbital injection of endothelial-targeted AAV (1×10^{11} viral particles/7.5 μL/mouse) for RAB5IF knockdown (RAB5IF-eKD#1/#2) was performed, followed by qRT-PCR (**J**) and Western blotting (**K**) analysis at P6 to assess knockdown efficiency of RAB5IF in mRMECs extracted from neonatal mice (pooled from 8 mice/sample, $n = 5$ samples/group, 15 μg protein/lane for WB). **L** IB4 staining of retinal flat mounts at P6, showing representative images, red box (magnified vascular structures), red dots (branching nodes), green box (magnified vascular front area), green arrows (tip cells), and yellow dots (filopodia). Quantification of vascular radial length, vascular density, branching nodes, number of tip cells, number of filopodia, and length of filopodia in RAB5IF-eKD and shC control groups of the neonatal mice ($n = 5$ mice per group). Scale bars =1 mm/60 μm. **M** Western blot of RAB5IF, CXCR4, and ESM1 in mRMECs from RAB5IF-eKD and shC mice at P6 (pooled from 8 mice/sample, $n = 5$ samples/group, 15 μg protein/lane for WB). Data are presented as means ± S.D.; One-way ANOVA with Bonferroni's post hoc test. Source data are provided as a Source Data file.

in both the number of sprouts and the average length of each sprout (Fig. 4B). RAB5IF silencing also impaired the proliferation of hRMECs, as indicated by a significant reduction in the ratio of EdU-positive nuclei (Fig. 4C). In addition, results from the Transwell migration assay demonstrated that the migratory capacity of hRMECs was compromised following RAB5IF silencing (Fig. 4D). The capillary tube formation assay further corroborated these findings, showing a significant reduction in tube-like structures formed by RAB5IF-silenced hRMECs (Fig. 4E). These results provide robust evidence that silencing RAB5IF induced an anti-angiogenic response in retinal endothelial cells.

To eliminate potential off-target effects associated with the previously utilized RAB5IF shRNAs and to further validate the role of RAB5IF in angiogenesis in vitro, we employed lentiviral CRISPR/Cas9 constructs designed to knockout RAB5IF. These constructs included sgRNAs targeting non-overlapping sequences in murine *RAB5IF* and were transduced separately into hRMECs. Following puromycin selection and *RAB5IF* KO screening, single stable cells, koRAB5IF#1 and koRAB5IF#2, were established. Western blotting analysis, Fig. 4F, confirmed the successful depletion of RAB5IF in these koRAB5IF hRMECs. Consistent with the phenotypic changes observed in cells expressing RAB5IF shRNA, CRISPR/Cas9-induced RAB5IF KO resulted in a significant reduction in both the number of sprouts and the average length of sprouting in hRMECs (Fig. 4G). Additionally, RAB5IF KO inhibited the proliferation and migration of hRMECs, as assessed through nuclear EdU staining (Fig. 4H) and Transwell migration assays (Fig. 4I), respectively. Moreover, RAB5IF KO compromised the tube-forming capacity of hRMECs (Fig. 4J). Thus, RAB5IF KO led to a pronounced anti-angiogenic response in hRMECs. Importantly, we assessed the impact of RAB5IF on two key energy metabolic pathways: oxidative phosphorylation (OXPHOS) and glycolysis, in hRMECs. Seahorse analysis demonstrated that both RAB5IF knockdown (via shRAB5IF#3) and KO (using koRAB5IF#1) resulted in a significant inhibition of OXPHOS (Fig. 4K), as the basal oxygen consumption rate (OCR) and maximum OCR as well as ATP production were decreased in RAB5IF-depleted hRMECs (Fig. 4K). Moreover, a significant reduction in the basal glycolysis and maximum glycolytic capacity was detected in RAB5IF-silenced/-KO hRMECs (Fig. 4L).

We also conducted a detailed investigation into the role of RAB5IF in mitochondrial function and morphology in hRMECs. Our findings indicated that knockdown of RAB5IF using shRAB5IF#3 decreased mitochondrial membrane potential, as evidenced by a marked decrease in Rhodamine 123 fluorescence intensity (Fig. S6A) and the accumulation of JC-1 green monomers (Fig. S6B). Immunofluorescence and electron microscopy analyses revealed that RAB5IF silencing led to decreased fusion of mitochondria, along with swelling and the loss or rupture of mitochondrial cristae (Fig. S6C, D). Overall, our results underscore the role of RAB5IF in regulating mitochondrial function and maintaining its morphology.

Contrarily, we investigated whether ectopic overexpression of RAB5IF could promote pro-angiogenic activity in hRMECs. A lentiviral construct encoding RAB5IF cDNA was transduced into hRMECs, resulting in the establishment of two stable cell selections, designated as oeRAB5IF-Sl1 and oeRAB5IF-Sl2. *RAB5IF* mRNA and protein expression levels were significantly elevated in the oeRAB5IF hRMECs (Fig. 4M). Quantitative analysis from in vitro sprouting assays indicated that both the average number of sprouts and the average length of each sprout were markedly increased following RAB5IF overexpression (Fig. 4N). Furthermore, RAB5IF overexpression enhanced hRMEC proliferation, as evidenced by a higher ratio of EdU-positive nuclei (Fig. 4O), and augmented the migratory capacity of hRMECs (Transwell assays, Fig. 4P). The mitochondrial OXPHOS capacity, tested by the ATP production (Fig. 4Q), and glycolysis levels (Fig. 4R) were both enhanced in RAB5IF-overexpressed hRMECs. Therefore, these in vitro results further supported the pro-angiogenic activity of RAB5IF in endothelial cells.

Proteomic sequencing identifies SUMO2 as a key RAB5IF-dependent protein

To further understand the possible underlying mechanism of endothelial RAB5IF in promoting angiogenesis, we performed proteomic sequencing of shRAB5IF (by shRAB5IF#3) and shC control hRMECs to identify differentially expressed proteins (DEPs), followed by functional enrichment analysis (Fig. 5A–C). We identified a total of 170 downregulated proteins and 163 upregulated proteins, applying thresholds of an adjusted *P*-value < 0.05 and |Fold Change| > 1.5 (Fig. 5A). Functional enrichment analysis indicated that the upregulated proteins are enriched in endodermal cell differentiation and extracellular matrix (ECM)-receptor interaction (Fig. 5B), whereas the downregulated proteins are involved in small ribosomal subunit synthesis, glycolysis, pyruvate metabolism, and the TCA (tricarboxylic acid) cycle (Fig. 5C). Proteins related to ribosomal subunit synthesis were visualized (Fig. 5D). Western blotting further confirmed that RAB5IF knockdown led to decreased expression of the 40S ribosomal subunit core protein RPS23, along with reductions in several ribosome assembly/processing factors, such as RPS19BP1, UTP6, PWP2, WDR46, and HEATR1 (Fig. 5E).

Among the downregulated proteins, small ubiquitin-like modifier 2 (SUMO2) protein expression was identified as the most significantly downregulated (Fig. 5F). Western blotting assays revealed that the knockdown or knockout of RAB5IF resulted in a significant reduction of SUMO2 protein expression in hRMECs (Fig. 5G), while SUMO1 levels remained unchanged (Fig. 5G). Additionally, the similar SUMO2 protein decrease was obtained by in primary mRMECs of P17 OIR RAB5IF-eKD mice (Fig. 5H). No changes in *SUMO2* mRNA levels were observed (Fig. 5I). Polysome profiling in hRMECs showed that, after RAB5IF knockdown, 80S ribosomes failed to effectively bind mRNA and

https://doi.org/10.1038/s41467-025-66212-x

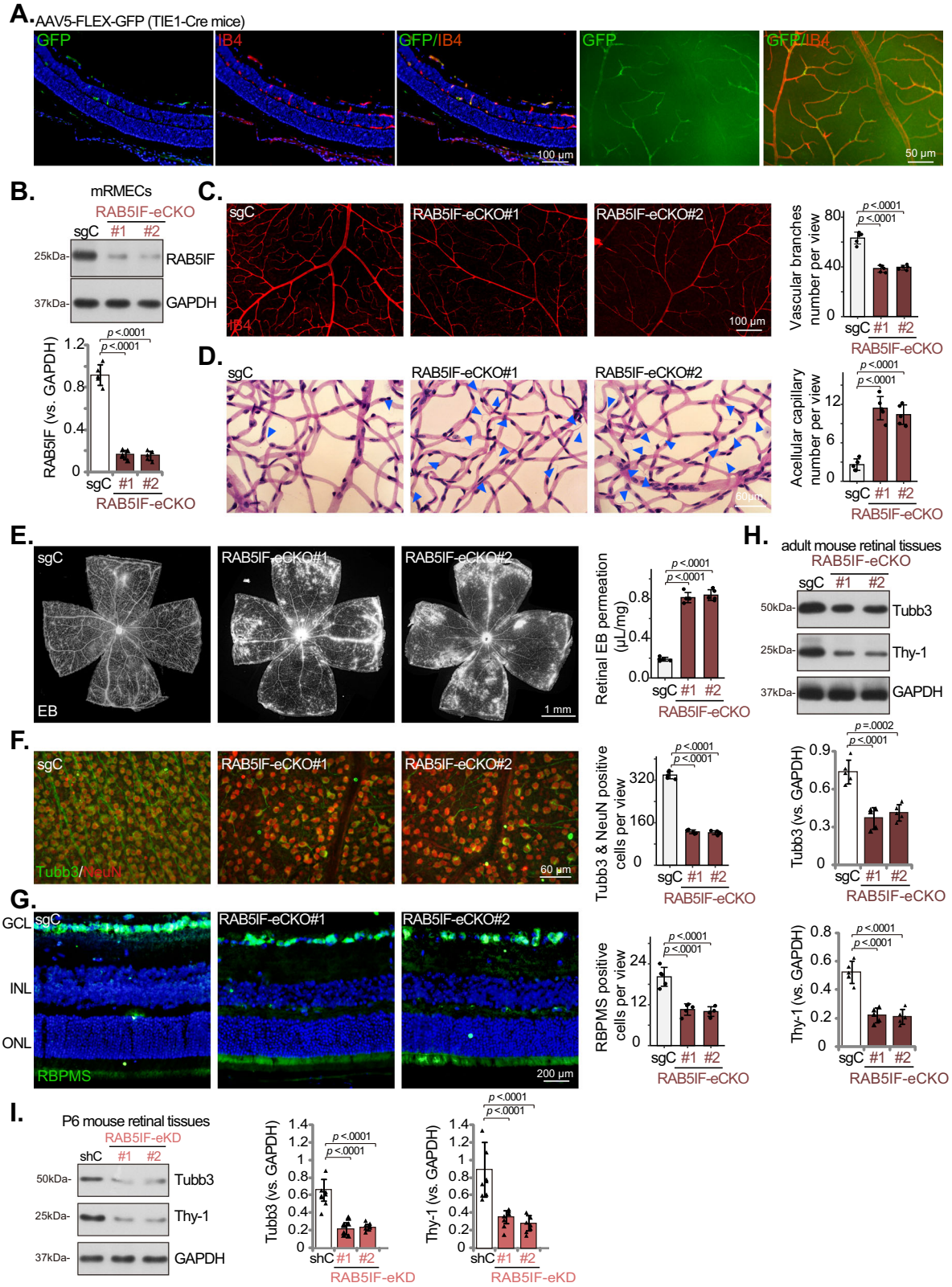

initiate translation, leading to the accumulation of 80S monomers and reduced polysomes, indicating inhibited translation initiation (Fig. 5J). Polysome PCR analysis indicated that RAB5IF knockdown selectively suppressed *SUMO2* mRNA translation without affecting *SUMO1* mRNA translation (Fig. 5K). Therefore, RAB5IF specifically upregulates SUMO2 protein in endothelial cells by selectively modulating the translation of SUMO2 *mRNA*.

Endothelial SUMO2 knockdown inhibits retinal neovascularization

Next, experiments were carried out to determine the possible role of SUMO2 in retinal neovascularization, we constructed shRNAs specifically targeting endothelial SUMO2 (SUMO2-eKD), which were again delivered via endothelial-targeted AAV(AAV^{ENT}-ICAM2p-shSUMO2) by retro-orbital injection. Two different SUMO2 shRNA with

Fig. 3 | Endothelial conditional knockout of RAB5IF inhibits retinal vasculature in adult mice. A The TIE1-Cre C57 mice (six-seven weeks old) were intravitreously injected with AAV5-FLEX-GFP viral particles (7×10^{10} viral particles/0.5 μL/mouse), followed by frozen sections and flat mount staining 21 days later to observe GFP-positive infection area. Scale bar = 100 μm / 50 μm. **B**–**H** The TIE1-Cre C57 mice (six-seven weeks old) were intravitreously injected with AAV5-FLEX-sgRAB5IF (RAB5IF-eCKO#1 and RAB5IF-eCKO#2, encoding non-overlapping sgRNAs against murine *RAB5IF*) or AAV5-FLEX-sgRNA control viral particles ("sgC), both at 7×10^{10} viral particles/0.5 μL/mouse; After 21 days RAB5IF protein expression in the primary mRMECs extracted from adult mice was shown (pooled from 4 mice/sample, $n = 5$ samples/group, 15 μg protein/lane for WB) (**B**); IB4 staining of retinal flat mounts, showing representative images, and quantification of vascular branch numbers. Scale bar = 100 μm (**C**). PAS staining of retinal tissue, showing representative images, and quantification of acellular capillary numbers. Scale bar = 60 μm (**D**). Evans blue (EB) leakage assay assessing retinal vascular leakage, showing representative images, and quantification of EB leakage. Scale bar = 1 mm (**E**). Tubb3/NeuN double staining of retinal flat mounts to label RGCs, showing representative images, and quantification of $Tubb3^+/NeuN^+$ cell numbers. Scale bar = 60 μm (**F**). RBPMS staining of retinal sections to label RGCs, showing representative images, and quantification of $RBPMS^+$ cell numbers. GCL, ganglion cell layer; ONL, outer nuclear layer; INL, inner nuclear layer. Scale bar = 200 μm (**G**). Expression of listed neuronal marker proteins in the retinal tissues was also tested (individual samples, $n = 5$ mice/group, 15 μg protein/lane) (**H**). **I** At P1, endothelial-targeted AAV (1×10^{11} viral particles/7.5 μL/mouse) was injected retro-orbitally for RAB5IF knockdown (RAB5IF-eKD). Subsequently, listed neuronal markers were detected by Western blot at P6. (pooled from 8 mice/sample, $n = 8$ samples/group, 15 μg protein/lane for WB). Data are presented as means ± S.D; One-way ANOVA with Bonferroni's post hoc test. $n = 5$ mice per group. Source data are provided as a Source Data file.

non-overlapping sequences were utilized, including SUMO2-eKD#1 and SUMO2-eKD#2. Compared to the control shRNA treatment (shC), the knockdown of SUMO2 in endothelial cells significantly inhibited retinal vascular development in neonatal mice, as evidenced by reductions in radial vascular length, vascular density, and the number of vascular branches (Fig. 6A). Additionally, this knockdown affected the tip cell phenotype, resulting in a marked decrease in the number of tip cells, as well as in the count and length of filopodia (Fig. 6A). Western blotting confirmed that SUMO2-eKD inhibited the expression of SUMO2 and tip cell markers CXCR4 and ESM1 in mRMECs from P6 neonatal mice, without affecting RAB5IF protein expression (Fig. 6B). Subsequently, we also examined SUMO2-eKD's effect in pathological retinal neovascularization (OIR model) and discovered that SUMO2-eKD had a pronounced inhibitory effect on pathological neovascular tufts (Fig. 6C). ELISA analysis showed that SUMO2-eKD did not alter the levels of VEGFA in the vitreous of P17 OIR mice (Fig. 6D). Additionally, in the OIR model, we investigated the localization of SUMO2 protein and discovered that SUMO2, similar to RAB5IF, was mainly expressed within the pathological neovascular tufts (Fig. 6E). These results suggest that RAB5IF's downstream protein SUMO2 is indeed important for pathological and physiological retinal neovascularization.

To investigate whether SUMO1 can compensate for SUMO2, we overexpressed SUMO1 in retinal endothelial cells via retro-orbital injection of AAV (AAV^{ENT}-ICAM2p-oeSUMO1) (Fig. S7A). In the OIR model, SUMO1-eOE failed to affect the inhibition of SUMO2-eKD on pathological retinal neovascularization (Fig. S7A). In vitro, using lentiviral vectors we generated SUMO2 knockdown (shSUMO2) hRMECs, with or without SUMO1 overexpression (+oeSUMO1) (Fig. S7B). SUMO2 silencing significantly impaired pro-angiogenic activity, evidenced by reduced tube formation and sprouting (Fig. S7C, D), which was not rescued by oeSUMO1 (Fig. S7C, D).

Endothelial SUMO2 knockdown inhibits retinal neovascularization reverses RAB5IF overexpression-facilitated retinal neovascularization

To determine whether SUMO2 is the critical downstream protein mediating the pro-angiogenic effects of RAB5IF, we tested whether silencing of SUMO2 could reverse RAB5IF-induced retinal neovascularization. We achieved RAB5IF overexpression in retinal endothelial cells through retro-orbital injection of AAV (AAV^{ENT}-ICAM2p-oeRAB5IF) in P1 mice. Results indicated that endothelial overexpression of RAB5IF (RAB5IF-eOE) significantly enhanced retinal vascular development by P6, characterized by significant increases in radial vascular length, vascular density, and the number of vascular branches (Fig. 6F). Furthermore, RAB5IF-eOE induced a substantial increase in the number of tip cells, as well as the length and quantity of filopodia (Fig. 6F). In primary mRMECs isolated from P6 neonatal mice, protein expression levels of both RAB5IF and SUMO2 were significantly elevated in RAB5IF-eOE mice (Fig. 6G). Importantly, SUMO2-eKD(#1) reversed the upregulation of SUMO2 in mRMECs from RAB5IF-eOE P6 mice without altering RAB5IF expression (Fig. 6G). In the oxygen-induced retinopathy (OIR) model, we similarly overexpressed RAB5IF (RAB5IF-eOE) in retinal endothelial cells through retro-orbital injection of same AAV at P3 mice. By P17 OIR, RAB5IF-eOE resulted in a significant increase in pathological neovascular clusters (Fig. 6H). These findings further substantiate the role of RAB5IF in promoting retinal neovascularization. Co-administration of AAV^{ENT}-ICAM2p-shSUMO2 (SUMO2-eKD#1) in the aforementioned RAB5IF-eOE mice completely reversed both physiological (P1-P6) and pathological (OIR) retinal neovascularization (Fig. 6F, H). These results suggest that SUMO2 is an essential downstream protein target of RAB5IF in mediating angiogenesis.

Conversely, we overexpressed SUMO2 in retinal endothelial cells through retro-orbital injection of AAV (AAV^{ENT}-ICAM2p-oeSUMO2) in RAB5IF-eKD mice. Notably, while SUMO2-eOE significantly increased SUMO2 mRNA levels in primary mRMECs of RAB5IF-eKD OIR mice (P17) (Fig. S8A), there was no significant increase at the protein level (Fig. S8B). This result strongly supports our proposed translational regulatory mechanism, where the absence of functional RAB5IF prevents the proper translation of *SUMO2* mRNA into protein, irrespective of mRNA availability. (see Fig. 5). In vitro, using lentiviral vectors we generated SUMO2 knockdown (shSUMO2) hRMECs with or without RAB5IF overexpression (oeRAB5IF) (Fig. S8C). shSUMO2 significantly impaired pro-angiogenic activity, evidenced by reduced tube formation and sprouting (Fig. S8D, E), which was not rescued by oeRAB5IF (Fig. S8D, E). These results further support that SUMO2 acts as the key downstream effector of RAB5IF in mediating its pro-angiogenic effect.

SUMO2-mediated SUMOylation of Gαi1/3 at both K92 and K277 is required for VEGF-induced signaling and pro-angiogenic activity

Since RAB5IF-driven angiogenesis is primarily mediated by promoting SUMO2 protein expression in endothelial cells, we explored the key protein targets that could possibly be SUMOylated by SUMO2. Importantly, both Gαi1 and Gαi3 proteins, two key signaling proteins important for endothelial cell functions and angiogenesis[18–22], were pulled down using anti-Flag magnetic beads (Fig. 7A), and mass spectrometry identified specific SUMO2 peptide segments within the complexes (Fig. 7A). Co-immunoprecipitation (Co-IP) experiments in HEK-293T cells confirmed that SUMO2-HA established an interaction with Gαi1-Flag and Gαi3-Flag (Fig. 7B). Additionally, SUMO2 protein associated with Gαi1 and Gαi3 in hRMECs (Fig. 7C, D).

After knockdown of SUMO2 using two different shRNAs, shSUMO2-1# and shSUMO2-2#, in hRMECs, no changes in Gαi1/3 protein levels were observed (Fig. 7E). It is therefore possible that SUMO2-mediated SUMOylation of Gαi1/3 may influence their interaction with other signaling proteins. Co-IP results indeed showed that SUMO2 knockdown hindered Gαi1/3's association with the receptor VEGFR2 and the key adaptor protein Gab1[22] in VEGF-treated hRMECs

https://doi.org/10.1038/s41467-025-66212-x

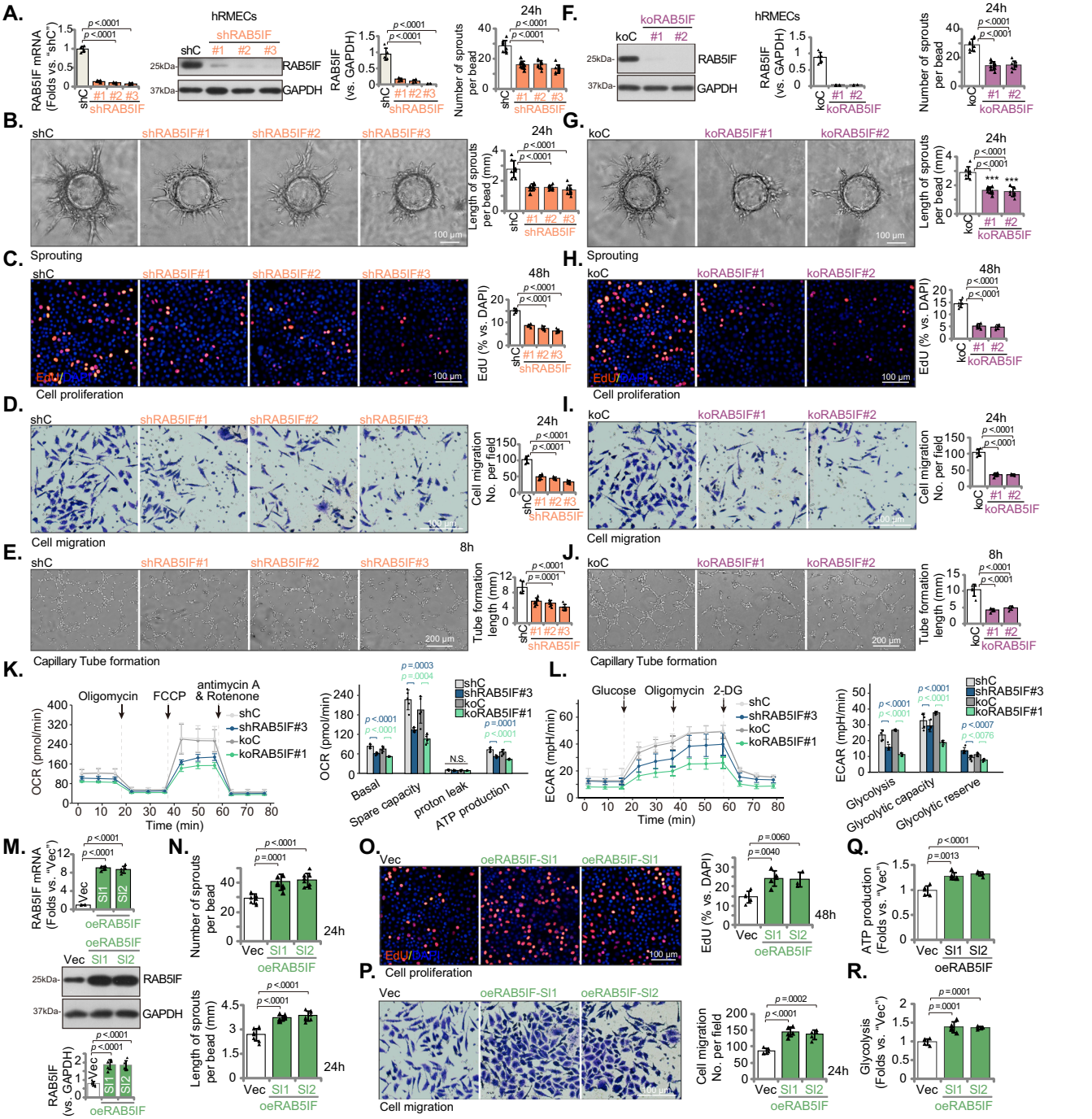

Fig. 4 | RAB5IF exerts significant pro-angiogenic activity in cultured retinal microvascular endothelial cells. A–E The human retinal microvascular endothelial cells (hRMECs) expressing the applied RAB5IF shRNAs (shRAB5IF#1, shRAB5IF#2 and shRAB5IF#3, with different shRNA sequences against *RAB5IF*) or the scramble control shRNA (shC) were established, expression of *RAB5IF* mRNA and protein was shown ($n = 5$ biological repeats, 15 μg protein/lane for WB) (**A**); Cells were further cultured for the indicated time periods, sprouting (**B**), cell proliferation (by testing EdU-positive nuclei ratio, **C**), migration (Transwell assays, **D**) and the capillary tube formation (**E**) were tested by the listed assays. **F–J** Stable hRMECs expressing the listed lentiviral CRISPR/Cas9-RAB5IF-KO construct (koRAB5IF#1/koRAB5IF#2, with different sgRNA sequences against *RAB5IF*) or the control construct with non-sense sgRNA (koC) were established, and RAB5IF protein expression was tested ($n = 5$ biological repeats, 15 μg protein/lane for WB) (**F**); Cells were further cultured for the indicated time periods, sprouting (**G**), cell proliferation (by testing EdU-positive nuclei ratio, **H**), migration (Transwell assays, **I**) and the capillary tube formation (**J**) and were tested. **K, L** Stable hRMECs with the designated genetic modifications on RAB5IF were cultured and subjected to Seahorse analyses to evaluate oxidative phosphorylation (**K**) and glycolysis (**L**). **M–R** Stable hRMECs with the lentiviral RAB5IF-expressing construct (oeRAB5IF-SI1/oeRAB5IF-SI2, two stable cell selections) or the empty vector (Vec) were established, expression of *RAB5IF* mRNA and protein was shown ($n = 5$ biological repeats, 15 μg protein/lane for WB) (**M**); Cells were further cultured for the indicated time periods, sprouting (**N**), cell proliferation (by testing EdU-positive nuclei ratio, **O**) and migration (Transwell assays, **P**) were tested, with results quantified. Seahorse assays were also carried out to evaluate ATP contents (**Q**) and basal glycolysis levels (**R**). Data are presented as means ± S.D., $n = 5$ (biological repeats). "N.S." indicates no statistical difference ($P > 0.05$); One-way ANOVA with Bonferroni's post hoc test. Scale bars = 100/200 μm. Source data are provided as a Source Data file.

https://doi.org/10.1038/s41467-025-66212-x

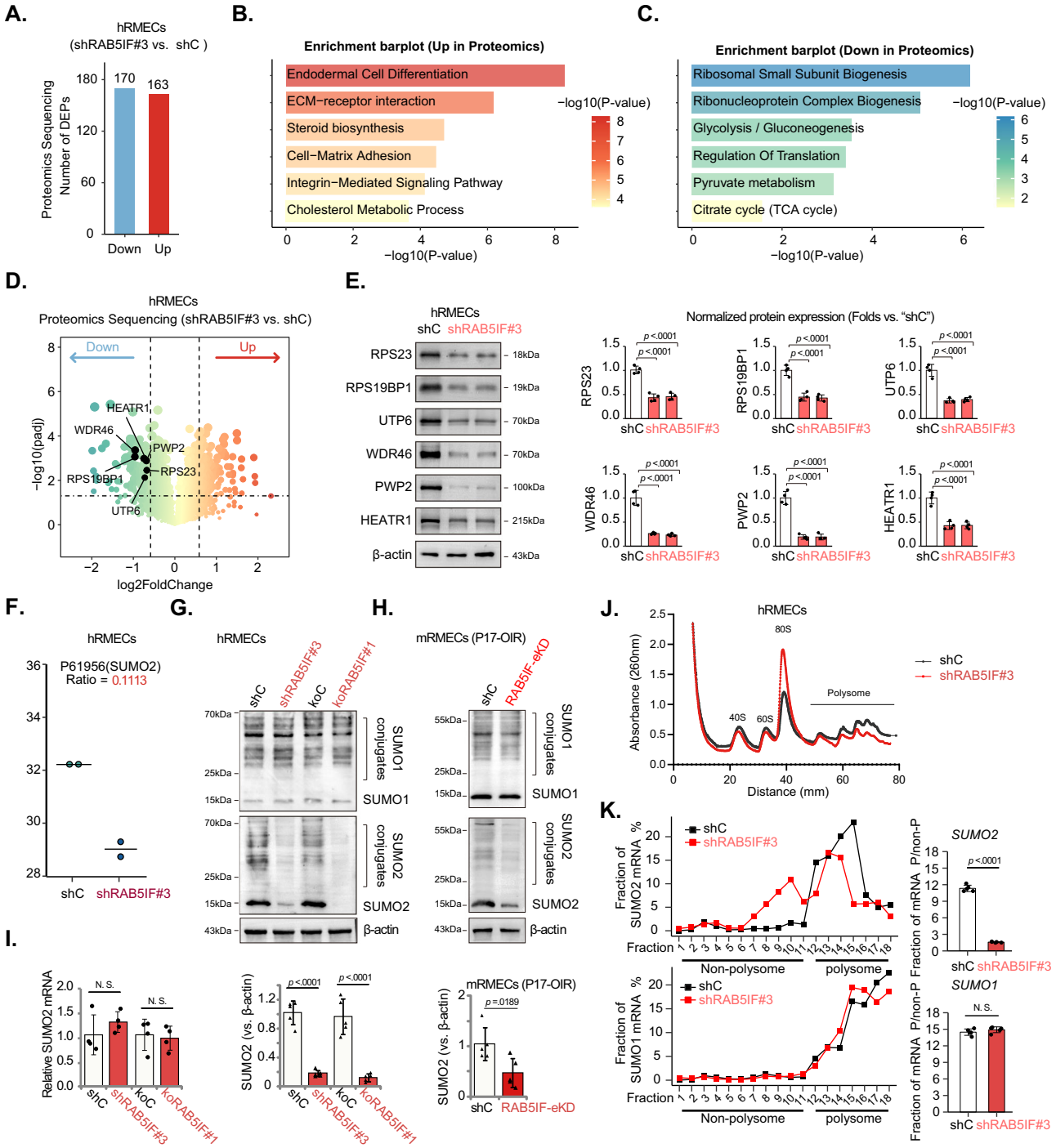

Fig. 5 | Proteomic sequencing identifies SUMO2 as a key RAB5IF-dependent protein. A–**F** Proteomic sequencing was performed on hRMECs with shRAB5IF (shRAB5IF#3) or shC, with volcano plots shown differentially proteins (**A**) ($n = 3$ biological repeats/group); GO functional analysis for the upregulated proteins (**B**) and downregulated proteins (**C**). Volcano plots showing differentially expressed proteins involved in ribosomal subunit synthesis (**D**). Expression of listed ribosomal proteins was also tested ($n = 4$ biological repeats, 15 μg protein/lane) (**E**). Scatter graph displaying SUMO2 as the top downregulated protein following RAB5IF silencing in hRMECs (**F**), with the center line marking the median ($n = 2$ biological repeats, a replicate was excluded due to non-detection of the SUMO2 protein). **G** Western blotting analysis of SUMO1 and SUMO2 protein expression following RAB5IF knockdown (shRAB5IF) or RAB5IF knockout (koRAB5IF) in hRMECs ($n = 5$ biological repeats, 15 μg protein/lane for WB). **H** Western blotting analysis of SUMO1 and SUMO2 protein expression in mRMECs extracted from RAB5IF-eKD and shC groups in P17 OIR mice (pooled from 4 mice/sample, $n = 5$ samples/group, 15 μg protein/lane). **I** qRT-PCR analysis of *SUMO1* mRNA expression following RAB5IF knockdown (by shRAB5IF#3) or RAB5IF knockout (by koRAB5IF#1) in hRMECs ($n = 5$ biological repeats). **J** Polysome profiling of shRAB5IF or shC. The x-axis represents the sucrose concentration gradient, and the y-axis shows OD260, reflecting mRNA levels ($n = 5$ biological repeats). **K** Polysome PCR analysis of *SUMO1* and *SUMO2* mRNA expression in shRAB5IF or shC hRMECs. The P/non-P ratio indicates overall translation activity ($n = 5$ biological repeats). Data are presented as means ± S.D; Fisher's exact test (**B**, **C**), One-way ANOVA with Bonferroni's post hoc test (**E**) and Two-tailed Student's t-test (**D**, **G**, **K**). Source data are provided as a Source Data file.

https://doi.org/10.1038/s41467-025-66212-x

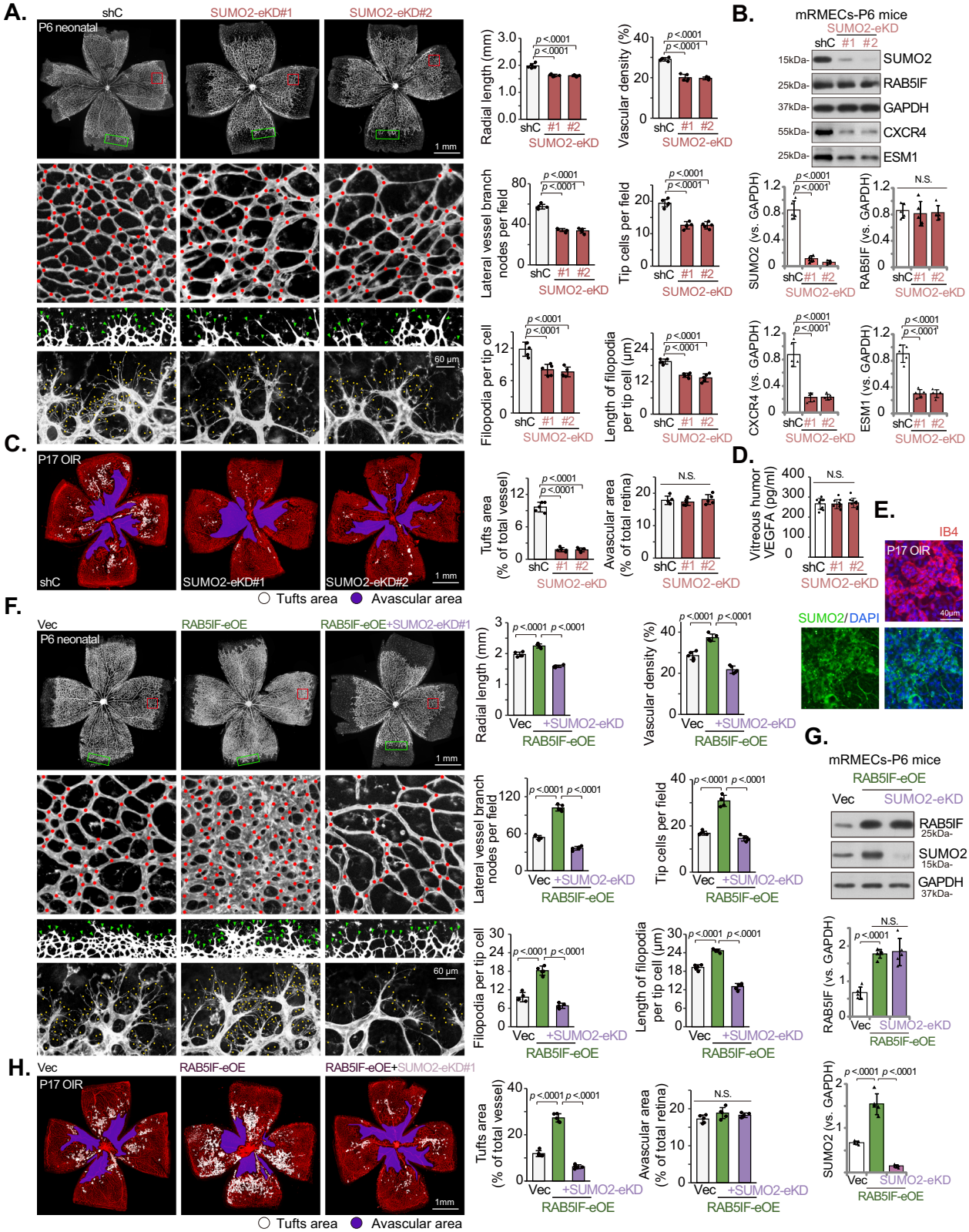

(Fig. 7F). As a result, phosphorylation levels of VEGFR2-Gαi1/3 downstream targets, including Akt, S6K, and Erk1/2, were substantially decreased (Fig. 7G). These findings suggest that SUMO2-mediated SUMOylation of Gαi1/3 is important for VEGFR2-Gαi1/3-Gab1 complex formation and VEFGR2 signaling transduction.

To further pinpoint the SUMOylation sites of Gαi1/3, we utilized JASSA and SUMOplot™ analysis tools to predict potential SUMOylation sites. This analysis identified two highly-conserved sites: lysine 92 (K92) and lysine 277 (K277) for both Gαi1 and Gαi3 (Fig. S9A–C). Using the CRISPR/Cas9 method, we successfully generated Gαi1 and Gαi3 double knockout (dKO) hRMECs (Fig. 7H). Next, we transfected Gαi1/3-dKO hRMECs with plasmids overexpressing wild-type, single-site Gαi1 and Gαi3 mutants (K92R and K277R), and double-site mutant (dKR) Gαi1 and Gαi3 proteins. Co-IP assays revealed that both K92R and

Fig. 6 | Endothelial SUMO2 knockdown inhibits retinal neovascularization, and reverses RAB5IF overexpression-facilitated retinal neovascularization. A, **B** At P1, endothelial-targeted AAV (1×10^{11} viral particles/7.5 μL/mouse) carrying SUMO2 shRNA (SUMO2-eKD#1/#2) was injected. Different shRNA sequences were utilized: SUMO2-eKD#1 and SUMO2-eKD#2) was performed. The IB4 staining of retinal flat mounts at P6, showing representative images. The red box (magnified vascular structures), red dots (branching nodes), green box (magnified vascular front area), green arrows (tip cells) and yellow dots (filopodia). Quantifications of vascular radial length, vascular density, branching nodes, number of tip cells, number of filopodia, and length of filopodia in P6 neonatal mice were shown ($n = 5$ mice per group). Scale bars = 1 mm/60 μm (**A**). Western blotting of listed proteins in primary mRMECs from P6 mice (pooled from 8 mice/sample, $n = 5$ samples/group, 15 μg protein/lane) (**B**). **C**–**E** At P3, mice received the same AAV injections and were subjected to OIR induction. At P17, IB4 staining revealed neovascular and non-perfused areas, quantified across groups ($n = 5$ mice per group) (**C**). Scale bar = 1 mm. ELISA analysis of VEGFA levels in the vitreous in P17 OIR mice ($n = 10$ mice per group) (**D**). Immunofluorescence of SUMO2 protein expression in pathological neovascular areas of P17 OIR mouse retinas (**E**). Scale bar = 40 μm. **F**, **G** At P1, AAV was injected to overexpress RAB5IF (RAB5IF-eOE) alone or combined with SUMO2 knockdown (SUMO2-eKD#1). At P6, IB4-stained flat mounts were analyzed for vascular parameters as above ($n = 5$ mice per group). Scale bars = 1 mm/60 μm (**F**). Western blotting of mRMECs confirmed protein expression (pooled from 6 mice/sample, $n = 5$ samples/group, 15 μg protein/lane) (**G**). **H** At P3, the same treatments were applied followed by OIR induction. At P17, IB4 staining was performed to assess and quantify neovascular and non-perfused areas ($n = 5$ mice per group). Scale bar = 1 mm. Data are presented as means ± S.D. "N.S." indicates no statistical difference ($P > 0.05$); One-way ANOVA with Bonferroni's post hoc test. Source data are provided as a Source Data file.

K277R mutations inhibited Gαi1/3 binding to SUMO2 (Fig. 7H), while dKR nearly completely blocked their interaction (Fig. 7H). These results indicated that both K92 and K277 are critical SUMOylation sites for Gαi1 and Gαi3.

Moreover, we assessed the impact of overexpressing wild-type and mutant Gαi1/3 proteins on VEGF-induced downstream signaling and in vitro angiogenesis. VEGF-induced Akt, S6K, and Erk1/2 phosphorylation was potentiated by Gαi1/3-WT in hRMECs (Fig. 7I). Whereas single-site Gαi1/3 (K92R or K277R) mutants weakened its effect (Fig. 7I), and Gαi1/3 dKR almost blocked it completely (Fig. 7I). The sprouting assay demonstrated that, upon VEGF stimulation, Gαi1/3-WT significantly enhanced endothelial cell sprouting; While single-site single-site Gαi1/3 (K92R or K277R) mutants inhibited this effect, and Gαi1/3-dKR (K92R and K277R) blocking it entirely (Fig. 7J). The capillary tube formation, Transwell, and nuclear EdU staining assays showed that Gαi1/3-WT potentiated VEGF-induced capillary tube formation, migration, and proliferation, while single-site Gαi1 and Gαi3 mutants (K92R and K277R) suppressed these effects (Fig. 7K–M), with dKR completely blocking them (Fig. 7K–M). Thus, SUMOylation of Gαi1 and Gαi3 at both K92 and K277, by the RAB5IF's protein target SUMO2, is required for VEGF signaling and pro-angiogenic activity.

SUMOylation of endothelial Gαi1/3 is required for retinal neovascularization in neonatal and OIR mice

To validate SUMOylation at the two conserved sites of Gαi1 and Gαi3 (K92and K277), which is important for angiogenesis in vivo, we constructed endothelial-specific AAV for overexpressing wild-type Gαi1/3 (Gαi1/3-WT-eOE) and the double-site mutant (Gαi1/3-dKR-eOE), both tagged with Flag. The AAV were delivered via retro-orbital injection at P1. Compared to the control vector (Vec), Gαi1/3-WT-eOE significantly enhanced retinal vascular development, as evidenced by increased radial vascular length, vascular density, and the number of vascular branches at P6 (Fig. 8A). This was accompanied by a marked increase in tip cells, with a noticeable rise in their number, filopodia count, and length (Fig. 8A), as well as enhanced expression of tip cell markers CXCR4 and ESM1 (Fig. 8B). The expression levels of the endogenous Gαi1 and Gαi3 (lower molecular weight) remained largely unchanged upon overexpression of the Flag-tagged dKR mutants or WT ones (Fig. 8C). In the OIR model, Gαi1/3-WT-eOE treatment at P3 also demonstrated a significant pro-angiogenic effect, resulting in a substantial increase in the area of pathological neovascular clusters at P17 OIR (Fig. 8D). In the contrast, the double-site mutants, Gαi1/3-dKR-eOE, failed to increase retinal neovascularization in neonatal and OIR mice (Fig. 8A–D). ELISA analysis showed that both Gαi1/3-eOE and Gαi1/3-dKR-eOE did not alter the levels of VEGFA in the vitreous of P17 OIR mice (Fig. 8E). These results suggest that SUMOylation at K92 and K277 of Gαi1/3 are required for their pro-angiogenic activity in vivo. Importantly, Western blotting analysis of P17 OIR retinal lysates demonstrated significantly higher protein expression of SUMO2 and Gαi1/3 specifically within the tufts area (pathological neovascularization) compared to the avascular area (Fig. S1A)

We investigated the signaling changes in the mRMECs derived from the aforementioned murine models. Our findings indicate a significant elevation in the activation of Akt (p-Akt), mTOR (p-S6) and Erk (p-Erk1/2) in the primary mRMECs of P17 OIR Gαi1/3-WT-eOE mice, compared to the vector control group (Fig. 8F). In contrast, the Gαi1/3-dKR-eOE mutants did not exhibit a statistically significant increase in Akt-mTOR activation within the mRMECs (Fig. 8F). In hRMECs overexpressing RAB5IF, specifically oeRAB5IF-Sl1 and oeRAB5IF-Sl2 (refer to Fig. 4), both SUMO2 protein expression and VEGF-induced Akt-S6K phosphorylation were markedly enhanced (Fig. 8G).

Increased vascular expression of RAB5IF and SUMO2 in fibrovascular membranes of proliferative diabetic retinopathy patients

At last, we analyzed RAB5IF and SUMO2 expression in proliferative diabetic retinopathy (PDR) patients. Utilizing the GSE60436 dataset, we investigated the expression of *RAB5IF* in fibrovascular membranes (FVMs) associated with both active and inactive PDR. Our analysis revealed no significant difference in *RAB5IF* expression in inactive FVMs; however, there was a marked upregulation of *RAB5IF* in active FVMs compared to normal retinal tissues (Fig. 9A). Additionally, GSE94019 dataset demonstrated a significant increase in *RAB5IF* expression in primary human retinal vascular endothelial cells (ECs) within FVMs, accompanied by elevated transcript levels of *SUMO1-3* (Fig. 9B). corroborate these findings, we examined clinical vitrectomy samples collected from our institution. The mean age of patients with macular epiretinal membranes (MEMs) and PDR was 60.50 ± 11.43 and 57.88 ± 6.90 years, respectively, showing no significant difference (two-tailed Student's t-test, $P = 0.5887$). Western blotting analysis revealed elevated protein levels of RAB5IF and SUMO2 in FVMs obtained from PDR patients (Fig. 9C), in contrast to MEMs from control patients (Fig. 9C). Furthermore, immunofluorescence analysis showed enhanced RAB5IF protein signals (in green fluorescence) in FVMs compared to MEMs (Fig. 9D, E), with fluorescence primarily localized to the vascular structures (IB4 staining) within the FVMs (Fig. 9D, E). Similarly, immunofluorescence staining for SUMO2 protein indicated stronger fluorescence in FVMs relative to MEMs, with pronounced SUMO2 signals within blood vessels in the FVMs (Fig. 9F, G). These results showed that RAB5IF and SUMO2 expression is increased in FVM of PDR patients.

Discussion

A comprehensive understanding of the molecular mechanisms governing aberrant angiogenesis in ocular tissues is essential for the development of innovative therapeutic approaches, including anti-VEGF treatments and gene therapies[1–3,24]. Mitochondria's multifaceted roles in energy metabolism, ROS signaling, and structural dynamics

https://doi.org/10.1038/s41467-025-66212-x

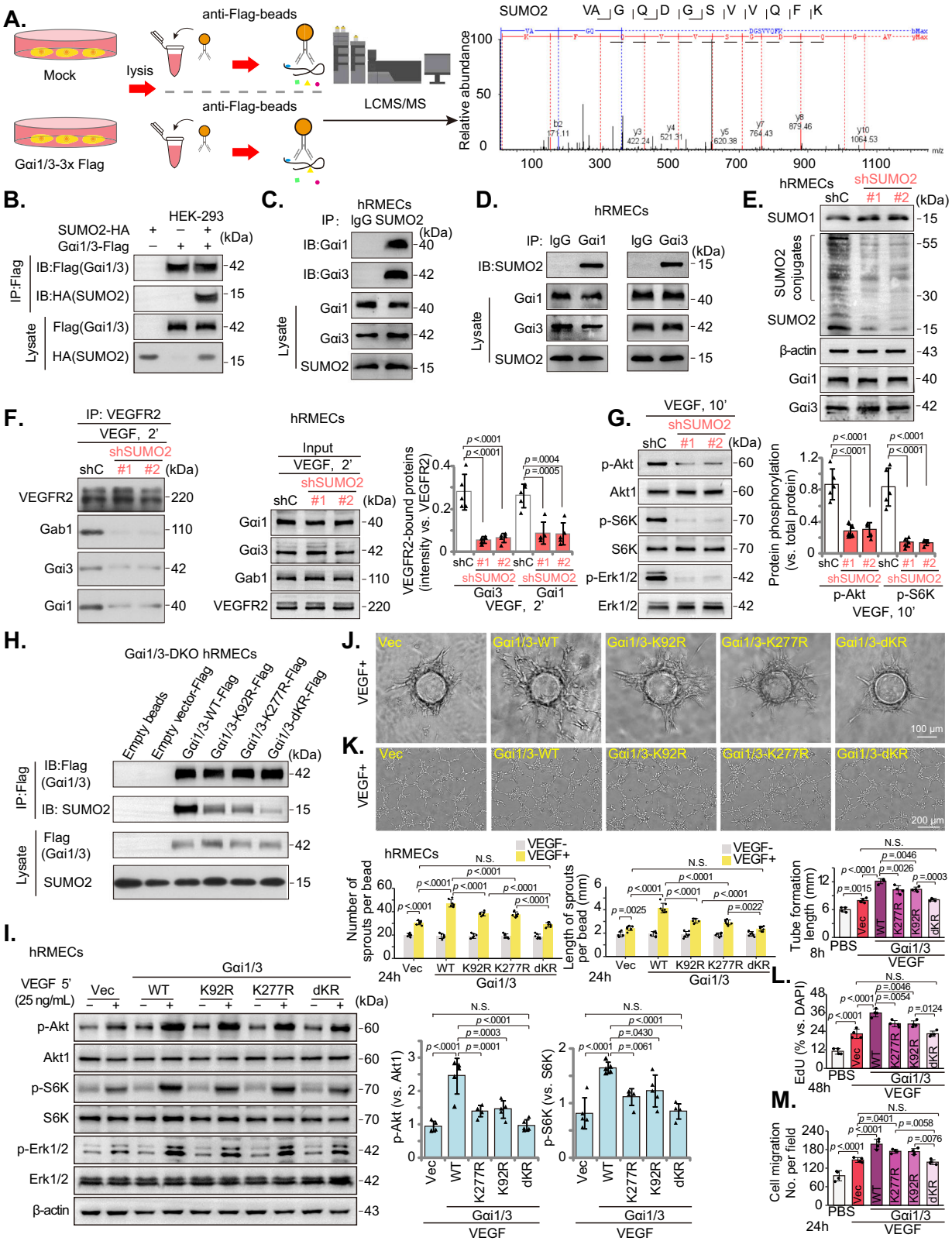

underscore their indispensable contribution to the complex and highly-regulated process of angiogenesis[12,25,26].

Early studies have highlighted the important roles of specific mitochondrial elements in angiogenesis. Wang et al. found that knockdown of the mitochondrial outer-membrane protein FUNDC1 (FUN14 domain-containing protein 1) in endothelial cells reduced VEGFR2 levels, negatively affecting capillary tube formation and spheroid sprouting in vitro, as well as angiogenesis in vivo[27]. In endothelial progenitor cells, inhibiting pyruvate kinase muscle isoenzyme 2 (PKM2) through C3k-mediated pathways led to downregulation of angiogenesis-related genes and suppressed capillary tube formation[28]. A recent study further demonstrated that genetic depletion of TIMM44 (translocase of inner mitochondrial membrane 44), a protein in the inner mitochondrial membrane[29], disrupted mitochondrial

Fig. 7 | SUMO2-mediated SUMOylation of Gαi1/3 at both K92 and K277 is required for VEGF-induced signaling and pro-angiogenic activity. A hRMECs were transduced with wild-type (WT) Gαi1 plus Gαi3 constructs (tagged with Flag), and stable cells were formed after puromycin selection. The anti-Flag magnetic beads were used for immunoprecipitation of Gαi1/3-Flag protein complexes, and SUMO2 peptides were identified through LC-MS/MS. **B**–**D** The co-immunoprecipitation (Co-IP) assays showed the association between SUMO2 and Gαi1/3 in HEK-293T cells (**B**) and hRMECs (**C**, **D**). ($n = 5$ biological repeats). **E**–**G** hRMECs were infected with lentivirus-packed SUMO2-shRNAs (shSUMO2-1# or shSUMO2-2#, representing two different sequences) or lentivirus-packed scramble control shRNA (shC), and stable cells established after puromycin selection. Expression of listed proteins tested (**E**); The above cells were also treated with VEGF (25 ng/mL) for designated time, and VEGFR2-Gab1-Gαi1/3 complex formation was tested via Co-IP assays (**F**), ($n = 5$ biological repeats); Expression of the listed signaling proteins was also tested (**G**). ($n = 5$ biological repeats, 15 μg protein/lane). **H** The Gαi1 plus Gαi3 double knockout hRMECs (Gαi1/3-DKO hRMECs) were further transduced with the designated wild-type (WT) or mutant Gαi1 plus Gαi3 constructs (tagged with Flag), stable cells were formed after puromycin selection, the association between SUMO2 and Flag-tagged Gαi1 plus Gαi3 as well as their expression levels were tested ($n = 5$ biological repeats). **I**–**M** The stable hRMECs with the designated wild-type (WT) or mutant Gαi1 plus Gαi3 constructs were treated with or without VEGF (25 ng/mL) for designated time, expression of listed protein was tested ($n = 5$ biological repeats, 15 μg protein/lane) (**I**); In vitro sprouting ability (**J**), capillary tube formation (**K**), cell proliferation (nuclear EdU staining assay) (**L**), and migration (Transwell assay) (**M**) were also examined, with results quantified. Scale bars, 100 μm for (**J**) and 200 μm for (**K**). Data are presented as means ± S.D. $n = 5$ (biological repeats). "N.S." indicates no statistical difference ($P > 0.05$); One-way ANOVA with Bonferroni's post hoc test. Source data are provided as a Source Data file.

functions in endothelial cells and impeded angiogenesis in vitro and in vivo. POLRMT (polymerase RNA mitochondrial transcription) is a mitochondrial enzyme responsible for synthesizing mitochondrial RNA. NDUFS8 (NADH: ubiquinone oxidoreductase subunit S8) is a component of the mitochondrial respiratory chain, specifically part of Complex I. Studies have shown that both are important for endothelial cell function and the process of angiogenesis[30,31].

RAB5IF is a mitochondrial protein that has garnered great attention recently[13]; however, its specific functions and roles within mitochondrial biology remain largely unexplored and poorly understood. The results of the present study suggest that endothelial RAB5IF is crucial for angiogenesis in vitro and in vivo. Analysis of single-cell RNA sequencing data and experimental verification demonstrated that *RAB5IF* is significantly increased in the retinal endothelial cells of OIR mice. Interestingly, RAB5IF, SUMO2, and Gαi1/3 were found to have significantly higher protein expression in the pathological neovascularization (tufts) of P17 OIR retinal lysates compared to the avascular area. This localized presence was supported by immunofluorescence, which showed strong RAB5IF protein signals specifically within neovascular tufts. Additionally, single-cell RNA sequencing data indicate that RAB5IF is predominantly expressed in the proliferating endothelial cells of P17 OIR mice, which are essential for pathological angiogenesis. These results suggest that targeting the RAB5IF-SUMO2-Gαi1/3 cascade may specifically inhibit pathological neovascularization and explain why its inhibition reduced tuft formation without affecting the central avascular area. This finding is consistent with previous OIR studies on interventions such as Akt inhibition[32], IL-33 silencing[33], Twist1 knockout[34], and valproic acid treatment[35], similarly reducing pathological neovascularization without significantly altering the avascular area.

RAB5IF is also significantly upregulated in choroidal endothelial cells during laser-induced CNV and knocking down RAB5IF in choroidal endothelial cells effectively suppressed pathological CNV. Furthermore, RAB5IF expression is elevated in mRMECs from P1 to P7 neonatal mice, and its knockdown hindered vascular development. RAB5IF eCKO also disrupted retinal vascular structure in adult mice. In vitro, depletion of RAB5IF through shRNA or CRISPR/Cas9 techniques significantly inhibited hRMEC sprouting, proliferation, migration, and capillary tube formation, while ectopic overexpression of RAB5IF elicited opposite effects, promoting these processes. Therefore, RAB5IF is a key mitochondrial protein required for endothelial cell function as well as physiological and pathological angiogenesis.

Arik and colleagues elucidated the critical role of glycolysis in the differentiation of tip cells[36]. Additionally, their findings indicate that both glycolysis and mitochondrial respiration (ATP production) are actively engaged during the proliferation of non-tip cells, as well as during sprouting angiogenesis, in both in vitro and in vivo settings[36]. Diebold et al. demonstrated that the depletion of a crucial subunit of the respiratory chain complex III, QPC, in endothelial cells leads to a significant reduction in cellular respiration, resulting in decreased endothelial cell proliferation and retinal angiogenesis in vivo[37]. It has been shown that VEGF elevated the expression levels of mitofusin 1 (MFN1) and mitofusin 2 (MFN2) in endothelial cells. This upregulation is crucial for the promotion of mitofusin, which is important for endothelial cell functions that underpin angiogenic processes[38]. Importantly, RAB5IF is important for mitochondrial respiration and morphology in endothelial cells. In RAB5IF-silenced or -KO hRMECs, oxygen consumption, ATP production, the maximum glycolytic capacity, and glycolysis ratio were all significantly reduced. Conversely, endothelial cells overexpressing RAB5IF exhibited elevated ATP levels and enhanced glycolytic capacity. Furthermore, shRNA-mediated silencing of RAB5IF resulted in mitochondrial depolarization and disrupted mitochondrial fusion in hRMECs. These results support an important role of RAB5IF in maintaining mitochondrial respiration and morphology in endothelial cells (see proposed signaling carton in Fig. 10).

One important finding of this study is that RAB5IF-mediated angiogenesis appears to occur through the upregulation of SUMO2 expression. Proteomic sequencing identified SUMO2 as a crucial downstream protein dependent on RAB5IF in endothelial cells. In cultured hRMECs, silencing or knockout of RAB5IF led to a marked reduction in SUMO2 protein levels, and its level was increased in RAB5IF-overexpressed endothelial cells. Furthermore, the endothelial knockdown of RAB5IF resulted in decreased SUMO2 protein expression in mRMECs derived from P17 OIR mice, whereas RAB5IF-eOE exerted opposite activity. RAB5IF silencing reduced the expression of RPS23, a core protein of the 40S ribosomal subunit, alongside several critical ribosome assembly and processing factors, including RPS19BP1, UTP6, PWP2, WDR46, and HEATR1. Polysome profiling revealed that RAB5IF knockdown prevented 80S ribosomes from effectively binding mRNA and initiating translation, resulting in an accumulation of 80S monomers and a reduction in polysomes, consistent with inhibited translation initiation. Furthermore, polysome PCR analysis demonstrated that RAB5IF knockdown selectively suppressed *SUMO2* mRNA translation. Therefore, RAB5IF depletion impedes ribosome biogenesis and translation initiation, specifically suppressing *SUMO2* mRNA translation and consequently lowering SUMO2 protein levels in endothelial cells. Notably, the endothelial knockdown of SUMO2 not only inhibited retinal neovascularization in both neonatal and OIR mouse models, but also reversed RAB5IF overexpression-facilitated retinal neovascularization in these contexts. These findings indicate that SUMO2 is a critical downstream protein target of RAB5IF in the regulation of endothelial cell function and angiogenesis. A more detailed mechanistic investigation of the specific translational regulation of SUMO2 by RAB5IF will be an exciting direction for future research.

SUMOylation, a post-translational modification involving the covalent attachment of SUMO proteins, plays a pivotal role in

https://doi.org/10.1038/s41467-025-66212-x

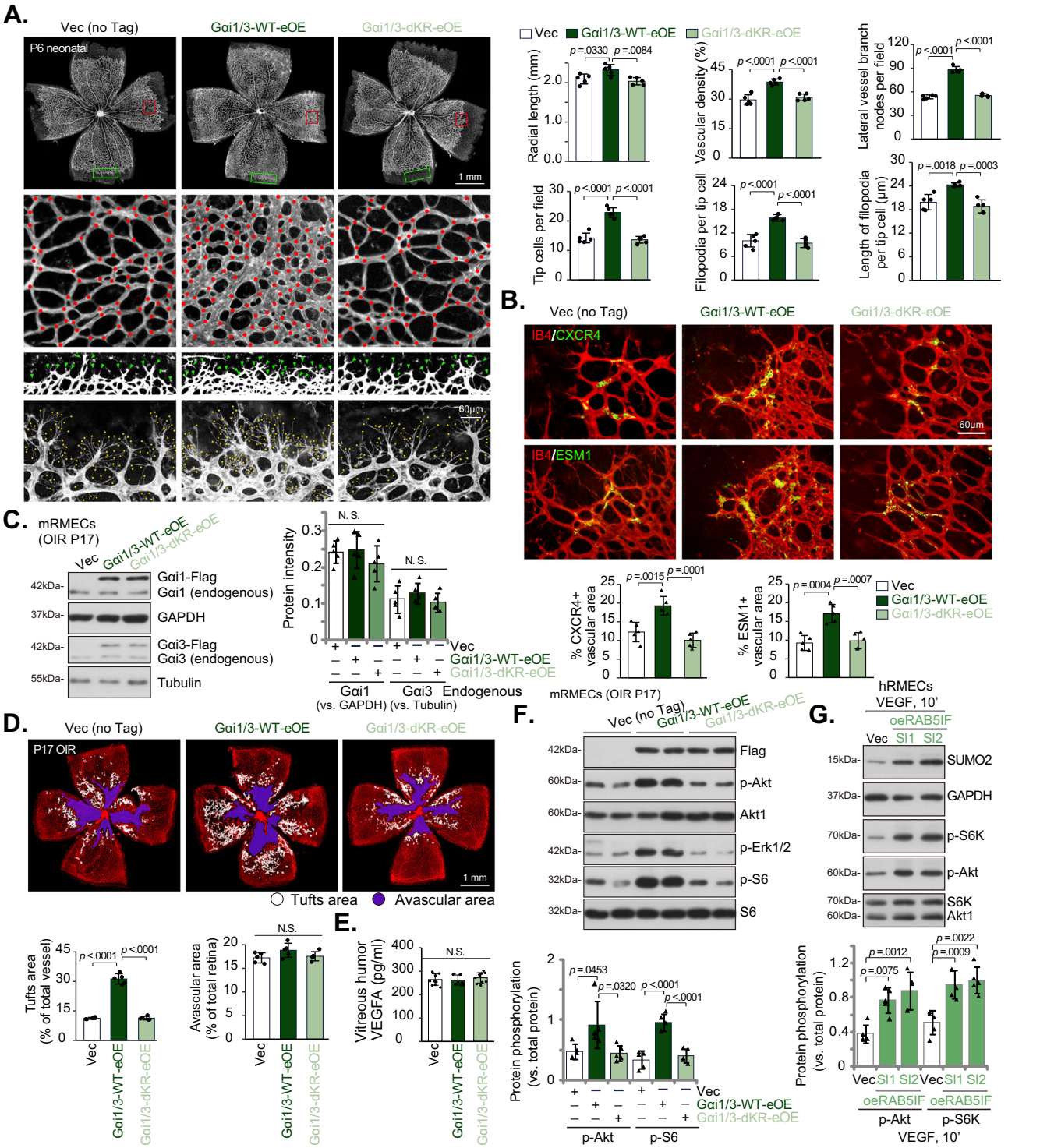

regulating angiogenesis. It is important for the activity, stability, and localization of various key pro-angiogenic factors. For instance, SUMOylation of hypoxia-inducible factor 1α (HIF-1α) at K391 and K477 enhances its transcriptional activity to enhance VEGF expression, thereby promoting endothelial cell proliferation, migration, and survival[39]. During pathological angiogenesis, SENP1 (small ubiquitin-like modifier protease 1)-mediated deSUMOylation of VEGFR2 is also important for its intracellular trafficking and signaling[40].

Previous studies in our group have demonstrated that Gαi proteins, specifically Gαi1 and Gαi3, serve as crucial signaling molecules that mediate the activation of the Akt-mTOR signaling cascade in response to both receptor tyrosine kinases (RTKs)[22,41–45] and non-RTK receptors[46,47]. Gαi1 and Gαi3 are integral to maintaining endothelial cell function and promoting angiogenesis, as they associate with VEGFR2 and other receptors involved in pro-angiogenic signaling[18–22]. In this study, we demonstrate that SUMO2, the RAB5IF downstream protein target, mediates SUMOylation of Gαi1 and Gαi3, and this modification is essential for their functional roles in endothelial cells. Silencing of SUMO2 significantly impaired the association of Gαi1 and Gαi3 with VEGFR2 and Gab1, thereby inhibiting VEGF-induced Akt-mTOR and Erk1/2 signaling in hRMECs. SUMO2 silencing did not alter the expression of Gαi1 and Gαi3 in endothelial cells. Importantly, mutations at the proposed SUMOylation sites of Gαi1 and Gαi3 disrupted their interaction with SUMO2 and inhibited VEGF-induced

Fig. 8 | SUMOylation of endothelial Gαi1/3 is required for retinal angiogenesis in neonatal and OIR mice. A–C At P1, retro-orbital injection of endothelial-targeted AAV (1×10^{11} viral particles/7.5 μL/mouse) was performed to overexpress murine wild-type (Gαi1/3-WT-eOE) or double mutant (K92R, K277R) Gαi1/3 (Gαi1/3-dKR-eOE), both Flag-tagged. The IB4 staining of retinal flat mounts at P6, showing representative images. The red box (magnified vascular structures), red dots (branching nodes), green box (magnified vascular front area), green arrows (tip cells) and yellow dots (filopodia) were shown (**A**). Quantifications included radial length, vascular density, branching nodes, tip cell number, and filopodia features ($n = 5$ mice per group) (**A**). Scale bars = 1 mm/60 μm. Tip cell markers CXCR4 and ESM1 were assessed by immunofluorescence at the vascular front ($n = 5$ mice per group) (**B**). Scale bars = 60 μm. Expression of listed proteins in mRMECs of P17 OIR mice was shown, with endogenous Gαi1 and Gαi3 protein expression quantified (pooled from 4 mice/sample, $n = 5$ samples/group, 15 μg protein/lane) (**C**). **D–F** At P3, the same AAV injections were performed. Mice were then subjected to OIR treatment at P12, IB4 staining on P17 OIR mice showed representative images, along with quantification of neovascular area and non-perfused area in the mice ($n = 5$ mice per group). Scale bar = 1 mm (**D**). Vitreous VEGFA levels at P17 were measured by ELISA ($n = 10$ mice per group) (**E**). The primary mRMECs were isolated from P17 OIR mice for protein analysis (pooled from 6 mice/sample, $n = 5$ samples/group, 15 μg protein/lane) (**F**). **G** Stable hRMECs expressing RAB5IF (oeRAB5IF-Sl1/Sl2) or empty vector (Vec) were generated and treated with VEGF (25 ng/mL) for indicated times. Listed protein expression was examined ($n = 5$ biological replicates, 15 μg/lane). Data are presented as means ± S.D. "N.S." indicates no statistical difference ($P > 0.05$); One-way ANOVA with Bonferroni's post hoc test. Source data are provided as a Source Data file.

downstream signaling in hRMECs. Furthermore, these mutations also resulted in reduced sprouting, capillary tube formation, proliferation, and migration of hRMECs in response to VEGF. In in vivo models, overexpression of Gαi1 and Gαi3 augmented retinal neovascularization in both neonatal and OIR mouse models; conversely, the double-site mutants of Gαi1 and Gαi3 exhibited a markedly diminished effect. These findings underscore the critical role of SUMOylation, by the RAB5IF protein target SUMO2, in the functionality of Gαi1 and Gαi3 in VEGF signaling, endothelial cell function, and angiogenesis (see proposed signaling carton in Fig. 10).

OIR, AMD, and PDR are common ocular diseases characterized by abnormal angiogenesis[1–3,24]. RAB5IF expression is upregulated in endothelial cells within both OIR and AMD mouse models, as well as in FVM of PDR patients. This upregulation underscores the potential translational value of RAB5IF as a therapeutic target, suggesting that interventions aimed at modulating its expression or function could provide strategies for treating these sight-threatening ocular conditions associated with pathological vascular growth.

Methods

Clinical sample collection and ethics

Macular epiretinal membranes (MEM) and fibrovascular membranes (FVM) were collected from informed written consent patients undergoing vitrectomy for macular disease or proliferative diabetic retinopathy (PDR) at Nanjing Medical University Eye Hospital (Nanjing, China). Our study population was limited to patients with severe disease requiring surgical intervention, as patients with milder conditions were excluded. Patients with surgical contraindications or a history of significant ocular trauma or prior surgery were excluded. The specimen collection did not alter the standard procedure or add any patient risk. All procedures received approval from the Ethics Committee of Nanjing Medical University Eye Hospital. These procedures complied with the principles outlined in the Declaration of Helsinki and the Department of Health and Human Services Belmont Report. Clinical information for the participants is available in Table S2.

Animal welfare and Ethics

All animal experiments were conducted using C57BL/6 J mice purchased from Hangzhou Ziyuan Laboratory Animal Technology Co., LTD (Hangzhou, China). For studies involving adult mice, half male and half female were used. Neonatal mice (P1 to P7) utilized mixed-sex litters, as sex cannot be reliably determined at this age. Mice were maintained in a specific-pathogen-free (SPF) animal facility with a 12-hour light/dark cycle, at a controlled temperature (22 ± 2 °C) and humidity (50-60%), with ad libitum access to food and water. Animal protocols were approved by the Institutional Animal Care and Use Committee (IACUC) and the Ethics Committee of Nanjing Medical University Eye Hospital, adhering to international standards for ethical treatment of animals in research.

Reagents

Polybrene and puromycin were purchased from Sigma-Aldrich (St. Louis, MO). All antibodies used in this study are listed in Table-S1. The mouse VEGFA ELISA kit (BMS619-2) and anti-Isolectin B4 (I21413) was obtained from Invitrogen (Nanjing, China). Dulbecco's modified Eagle's medium (DMEM), antibiotics, serum, and other cell culture reagents were obtained from Gibco-BRL (Suzhou, China).

Cell culture

Human retinal microvascular endothelial cells (hRMECs, cat no. CP-H130) were procured from the Procell (Shanghai, China). All cell lines used in this study were authenticated by Short Tandem Repeat (STR) profiling and confirmed to be free of mycoplasma contamination. hRMECs was cultured in high glucose DMEM/F-12 medium (17.51 mM) supplemented with 10% fetal bovine serum (FBS). The cells were maintained at 37 °C in a humidified atmosphere containing 5% CO_2. To promote an angiogenic phenotype in vitro, the culture medium was supplemented with insulin (2.5 μg/mL), epidermal growth factor (EGF, 100 ng/mL), VEGF (2.5 ng/mL), and adenine (24 μg/mL)[18,21].

Processing and analysis of published sequencing data

Single-cell RNA sequencing datasets were obtained from the Gene Expression Omnibus (GEO), including OIR (oxygen-induced retinopathy) and age-matched control normoxia mouse retina data (GSE150703), postnatal day 6 (P6) and P10 mouse retina data (GSE175895), and age-related macular degeneration (AMD) patient versus normal control human choroid data (GSE135922[48]). The raw counts were processed in R using the Seurat v5 package, transforming each dataset into a Seurat object, followed by quality control to filter out low-quality cells based on feature counts (200 to 3000 features). Data normalization was performed to account for sequencing depth and technical variations, and UMAP (uniform manifold approximation and projection) plots were generated to visualize clustering results, with expression of *RAB5IF* assessed using feature plots. Endothelial cells were further annotated and clustered based on specific marker genes. Tip endothelial cells express high levels of classic tip markers (*VEGFR2*, *TP53I11*, *CXCR4*), Stalk ECs show high proliferation markers (*KI67*, *PCNA*, *TOP2A*), and Phalanx ECs express *VEGFR1* and *TIE1* without active tip or stalk markers[49,50]. Additionally, RNA-seq data from proliferative membranes of PDR (proliferative diabetic retinopathy) patients (GSE94019 and GSE60436) were utilized to analyze *RAB5IF* expression through differential expression analysis using the limma package, with results visualized via a volcano plot.

Gene silencing or knockout (KO) in vitro and in vivo

For in vitro studies, lentiviral short hairpin RNAs (shRNAs) and single guide RNAs (sgRNAs) obtained from Shanghai Genechem Co. (Shanghai, China) were utilized for gene knockdown and knockout (KO) in hRMECs. The vector employed for the delivery of lentiviral

https://doi.org/10.1038/s41467-025-66212-x

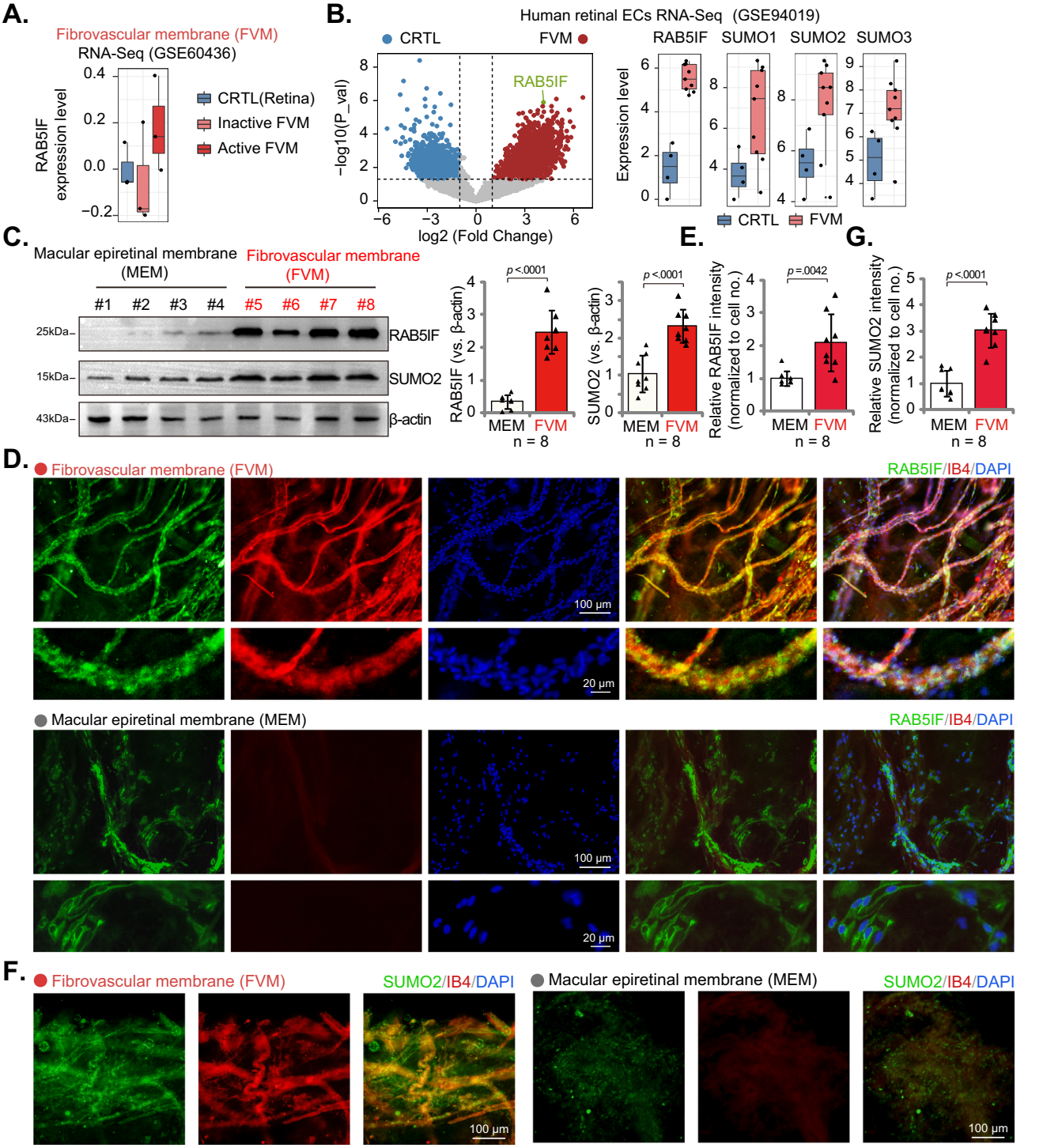

Fig. 9 | Increased vascular expression of RAB5IF and SUMO2 in fibrovascular membranes of proliferative diabetic retinopathy patients. A RNA-seq data (GEO: #GSE60436) showing the expression of *RAB5IF* in healthy human retinas, inactive PDR fibrovascular membranes, and active PDR fibrovascular membranes (individual samples, $n = 3$ tissues/group). The box plot displays the median (center line), interquartile range (IQR; box limits), and 1.5 × IQR whiskers. **B** RNA-seq data (GEO: #GSE94019) displaying the expression of *RAB5IF* and *SUMO1-3* in primary retinal vascular endothelial cells extracted from healthy human retinas and PDR fibrovascular membranes (individual samples, $n = 4$ tissues in CTRL group, $n = 9$ tissues in FVM group). The box plot displays the median (center line), IQR (box limits), and 1.5 × IQR whiskers ($n = 3$ biological repeats). **C** Western blotting analysis and quantification of RAB5IF and SUMO2 protein expression levels in the described macular epiretinal membrane (MEM) and fibrovascular membrane (FVM) tissues (individual samples, n=8 tissues/group, 15μg protein/lane). **D**–**F** Immunofluorescence of RAB5IF (**D**, **E**) and SUMO2 (**F**, **G**) proteins in the described macular epiretinal membrane (MEM) and fibrovascular membrane (FVM) tissue sections, along with vascular staining (IB4). Scale bars = 100/20 μm. ($n = 8$ tissue slides per group). Data are presented as means ± S.D.; two-tailed Student's t-test (**B**, **C**, **E**, and **G**). Source data are provided as a Source Data file.

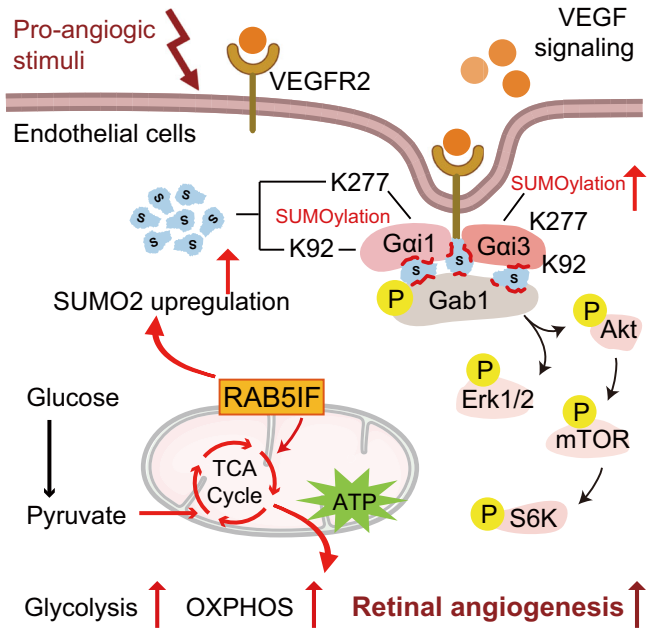

Fig. 10 | The proposed signaling pathway of this study. RAB5IF promotes pathological and developmental retinal angiogenesis, potentially through promoting mitochondrial respiration and fusion, as well as increasing SUMO2 protein expression. The latter also promotes SUMOylation of Gαi1 and Gαi3, which is vital for mediating VEGFR signaling.

shRNA in vitro was GV493 (hU6-MCS-CBh-IRES-puromycin, devoid of GFP), while the vector for lentiviral sgRNA-mediated gene knockout was GV708 (U6-sgRNA-EF1a-Cas9-FLAG-CMV-P2A-puromycin, also no GFP). Lentivirus production was achieved by transducing the aforementioned constructs along with lentiviral packaging constructs into HEK-293 cells. The endothelial cells were plated in six-well plates at 50-60% confluence in complete medium supplemented with polybrene, and subsequently infected with lentivirus at a multiplicity of infection (MOI) of 10-11. Following a 24 h incubation, the cells were cultured in complete medium containing puromycin (3.0 μg/mL) for an additional 5-6 passages to select for successfully transduced stable cells. The efficacy of gene silencing or KO in the stable cell populations was confirmed through Western blotting and/or qRT-PCR (quantitative reverse transcription polymerase chain reaction) assays. Control cells received lentivirus encoding a non-sense scramble control shRNA ("shC", Genechem) or non-sense sgRNA ("sgC", Genechem). Double knockout (DKO) of Gαi1 and Gαi3 in cultured endothelial cells expressing Cas9 and stable cell establishment via CRISPR/Cas9-KO lentiviral constructs, which respectively carried the puromycin resistance marker. Gαi1 and Gαi3 DKO was subsequently achieved through puromycin selection, single-cell cloning, and verification via Western blotting assays in the stable cells. For in vivo studies, adeno-associated viruses (AAV) sourced from Shanghai Genechem Co. were engineered to express specific shRNA sequences constructs. These AAV utilized an endothelial-specific promoter, intercellular adhesion molecule 2 (ICAM2), in conjunction with a high-transduction serotype (AAV^{ENT}-ICAM2p), thereby facilitating targeted delivery to retinal endothelial cells in vivo. For the neonatal mouse and OIR models, retro-orbital AAV injection used a dose of 1×10^{11} viral particles/7.5 μL/mouse, and for the CNV model, intravitreal AAV injection used a dose of 1×10^{12} viral particles/0.5 μL/mouse. To generate RAB5IF endothelial conditional knockout (RAB5IF-eCKO) mice, AAV5-FLEX-sgRAB5IF constructs from Genechem Co. were engineered to express two different sgRNA sequences targeting murine *RAB5IF*. These two constructs were respectively administered via intravitreal injection at a dose of 7×10^{10} viral particles/0.5 μL/mouse into adult TIE1-Cre C57BL/6 J mice (as reported previously[21]), resulting in the successful establishment of RAB5IF-eCKO mice after 21 days. These mice contain a ubiquitous, floxed *Cas9* allele and the TIE1-Cre transgene. Upon intravitreal injection of AAV5-FLEX-sgRAB5IF constructs, Cas9 expression is conditionally activated via Cre-mediated recombination exclusively in TIE1-expressing endothelial cells. This activated Cas9, guided by the AAV, then precisely targets the RAB5IF gene within these specific cells. The methodology for the intravitreal injection of AAV has been detailed in our previous study[21]. The targeted sequences utilized were listed in Table-S3. T7 endonuclease I (T7E1) cleavage assay and Sanger sequencing of target DNA Loci were utilized to confirm successful gene *RAB5IF* editing. Western blot assays were carried out to verify the knockout of the target protein.

Gene overexpression

For in vitro studies, the pcDNA3.1-3xFlag constructs, which encode both wild-type (WT) or mutant Gαi1 and Gαi3 proteins (murine and human), were acquired from Suzhou Genepharma Co. (Suzhou, China). The lentiviral GV492 constructs (Genechem, Shanghai, China), which harbors the RAB5IF-expressing sequence, SUMO1-expressing sequence or SUMO2-expressing sequence, were provided by Genechem. Lentivirus was produced by transducing HEK-293 cells with the constructs and virus packaging components. Cells were plated at 60% confluence in complete medium with polybrene and infected with lentivirus at MOI of 10-11. After 24 h, they were cultured in puromycin (3.0 μg/mL) medium for 5-6 passages to select stable cells. The efficacy of gene expression was confirmed via Western blotting and/or qRT-PCR assays. Control cells were infected with a lentiviral empty vector construct. For in vivo studies, AAV sourced from Shanghai Genechem Co. were engineered to express cDNA of targeted genes (*SUMO1*, *SUMO2*, *RAB5IF*, *Gαi1* or *Gαi3*). These AAVs again utilized an endothelial-specific promoter, AAVENT-ICAM2p. The AAV were administered to retinal tissues through retro-orbital injection. For control treatment, an AAV-packed vector control was administered.

Retro-orbital injection

For retro-orbital injection, a 31-gauge needle attached to a 0.3-mL syringe (BD Ultra-Fine II 8 mm needle, Shanghai, China) was utilized on adult mice anesthetized[21], while pups were manually restrained without anesthesia. The needle, bevel facing downward, was inserted into the eye socket at the "three o'clock" position at an angle of approximately 30°, with successful entry into the sinus confirmed by drawing back the syringe plunger to observe blood.

Oxygen-induced retinopathy (OIR)

The newborn mouse pups (P7) were raised with nursing mothers and exposed to 75 ± 1% oxygen from P7 to P12. Following the oxygen exposure, the pups were returned to normal room air (21% oxygen) for an additional 5 days (P12 to P17). Upon reaching P17, mice were anesthetized and euthanized via cervical dislocation, followed by retinal dissection and vascular staining. The stained retinal flat mounts were used to assess the area of neovascularization and the area of non-perfusion. The purple-shaded areas denote the avascular (non-perfused) regions, while white areas denote the pathological neovascular tufts. Neovascularization percentage = (neovascular area / total flat mount area) × 100%; Non-perfusion percentage = (non-perfused area / total flat mount area) × 100%. To separate tufts and avascular regions, P17 OIR mouse retinas (without PFA fixation) were flat-mounted and positioned with the inner surface up in a Sylgard-coated petri dish under a fluorescence dissecting microscope after systemic IB4 staining. Using the IB4 fluorescence as a guide, precise microdissection was performed to isolate the neovascular tufts and the central avascular regions. The excised tissue samples were immediately transferred to pre-chilled microcentrifuge tubes containing RIPA lysis buffer with protease inhibitors, snap-frozen on dry ice, and then

stored at −80 °C until further protein extraction and Western blot analysis.

Retinal vascular development

As reported previously[21], neonatal mice were utilized to study retinal blood vessel development. On postnatal day 6 (P6), pups (half male, half female) were anesthetized, euthanized by cervical dislocation, and their retinas were dissected and stained. Endothelial-targeting AAV was injected retro-orbitally on postnatal day 1 (P1), with eyes harvested for analysis at P6. Stained retinal flat mounts allowed the assessment of parameters such as radial length (measured from the center to the farthest point of the vessels), vascular density (ratio of vascular area to total area), number of branching nodes (manually counted), number of tip cells (manually counted at vessel ends), as well as the number and lengths of filopodia (photographed, counted, and measured from base to tips).

Laser-induced choroidal neovascularization (CNV) model

The laser-induced CNV model was established using photocoagulation in 7–8-week-old C57BL/6 J mice (half male half female). After anesthetizing and dilating their pupils with 1% tropicamide (Alcon, Geneva, Switzerland), laser photocoagulation (Quantel Medical, Clermont-Ferrand, France, 577 nm) was applied at three, six, nine, and twelve o'clock positions surrounding the optic discs bilaterally, utilizing a slit lamp delivery system with a coverslip as a contact lens. The laser (75 μm diameter, 100 ms duration, 100 mW) disrupted Bruch's membrane, confirmed by immediate subretinal bubble formation; sites without bubbles were excluded. Endothelial-targeting AAV particles were injected intravitreally 21 days prior to laser induction, and the eyes were harvested 7 days later. The CNV area was quantified through choroidal flat mounts stained with isolectin B4 (IB4). Eyes are collected and fixed in 4% paraformaldehyde (PFA) for 30 min, followed by careful enucleation and dissection to separate the retina and choroid, which are then placed on glass slides for immunofluorescence analysis to evaluate vascular structures.

Ex vivo choroidal explant culture

Adult C57BL/6 J mice were euthanized by CO_2 asphyxiation followed by cervical dislocation. The eyes were promptly enucleated and immersed in ice-cold EBM (endothelial basal medium, Lonza, Basel, Switzerland) for dissection. The choroid was carefully excised and cut into explants measuring 1 × 1 mm^2. These explants were embedded in growth factor-reduced Matrigel (Corning, Corning, New York) mixed with endothelial growth medium-2 (EGM-2, Lonza) supplemented with 10% serum. Each explant was placed in a 24-well plate and incubated at 37 °C for 30 min. Afterward, each well was filled with 500 μL of medium and incubated at 37 °C. Images of the explants were captured at 3 to 5 days post-culture to assess vascular growth, and the sprouting area was quantified by measuring the extent of vascular outgrowth from each explant.

Immunofluorescence staining

The described tissues were fixed in 4% PFA for 30 min at room temperature, then permeabilized overnight at 4 °C in a PBS solution containing 1% Triton X-100 and 5% BSA (Biofroxx, Germany). They were subsequently incubated with primary antibodies at 4 °C for 12–48 h. For vascular staining, samples were stained with IB4 probe[21] at 4 °C for 2 h. Images were captured using a fluorescence microscope (Olympus, Japan). The antibodies utilized for the immunofluorescence assays were listed in Table-S4.

Extraction and primary culture of retinal or choroid vascular endothelial cells

Primary retinal and choroidal vascular endothelial cells were isolated by digesting retinas and choroids. For primary retinal vascular endothelial cells, retinas from 6-8 pups were minced and digested with 1 mg/mL collagenase I (Sigma, St. Louis, MO) at 37 °C for 45 min, filtered through a 45 μm strainer (Beyotime, Wuxi, China), and centrifuged at 90 × *g* for 5 min before re-suspension in the described endothelial basal medium. For primary choroidal vascular endothelial cells, the RPE (retinal pigment epithelium)-choroid-sclera complex tissues from 4–5 mice was pooled and treated with 0.05% trypsin (Thermo Fisher) at 37 °C for 15 min to detach RPE. The choroid-sclera complex was minced and digested with 2 mg/mL collagenase II (Biofroxx, Germany) and 30 U/mL DNase I (Beyotime, Wuxi, China) in serum-free medium at 37 °C for 60 min, with pipetting to aid dissociation. After filtering and centrifugation, choroidal cells were washed and resuspended in endothelial basal medium. Cell suspensions were purified using Dynabeads™ CD31 magnetic beads (Invitrogen, Suzhou, China) and approximately 2 × 10^5 viable cells cultured in endothelial basal medium on 0.2% w/v gelatin-coated 6-well plates for analysis.

Periodic acid-schiff (PAS) staining

Freshly enucleated eyes were fixed in 10% neutral formaldehyde for 24 h. The retina was then excised and incubated in 3% trypsin at 37 °C until the non-vascular components dissociated, creating a cloudy medium. The retina was gently agitated to release the vascular network, washed, and mounted on glass slides to dry. Vascular structures were stained using PAS-hematoxylin and examined under light microscopy. Images were analyzed to quantify the number of acellular capillaries.

Evans blue (EB) permeability assay

To evaluate retinal vascular permeability, EB dye (30 mg/kg) was administered intravenously via the femoral vein in adult mice. After 1 h, the mice were euthanized, and the ocular globes were fixed in 4% PFA for 30 min. The retinas were then dissected into four quadrants. Portions of the retinas were used for fluorescence microscopy to detect EB, while others were incubated overnight in dimethylformamide at 70 °C to extract the dye. The supernatant containing the extracted dye was analyzed spectrophotometrically, measuring absorbance at 620 nm for the blue signal and at 740 nm for background correction. The amount of EB leakage the retina was calculated based on the standard curve of EB.

In vivo retinal ganglion cells (RGCs) assessment

RGCs were quantified through NeuN (neuronal nuclear) plus Tubb3 (tubulin beta 3 class III) double staining in flat-mounted retinas and RBPMS (RNA binding protein with multiple splicing) staining in retinal cryosections. Detailed immunofluorescence procedures were outlined in the immunofluorescence section.

Cellular functional assays and gene/protein detection

Cellular assays were conducted to evaluate various functions in cultured endothelial cells, including cell proliferation via nuclear EdU (5-ethynyl-2′-deoxyuridine) staining, in vitro cell migration using "Transwell" assays, and endothelial cell capillary tube formation. Cell proliferation was assessed by nuclear EdU (5-ethynyl-2′-deoxyuridine) staining. Briefly, 5 × 10^4 cells were seeded in 24-well plates and stained using the EdU Kit (Byotime, Nanjing, China) according to the manufacturer's protocols. For Transwell assays, 1.5 × 10^4 genetically treated endothelial cells were added to each chamber. In the capillary tube formation assay, 1 × 10^5 cells were seeded onto pre-coated 24-well plates. Crystal violet dye was used to stain migrated cells and the length of the formed tubes was quantified utilizing the Angiogenesis Analyzer plugin in Fiji (ImageJ). For other fluorescence dye assays, hRMECs with specified genetic modifications were cultured at a density of 5 × 10^4 cells per well in 24-well plates for a duration of 24 h. Cells were then exposed to selected fluorescent dyes, including JC-1

(5,5′,6,6′-Tetrachloro-1,1′,3,3′-tetraethylbenzimidazolcarbocyanine iodide) and Rhodamine-123, at 37 °C for a period ranging from 20 to 30 minutes. Subsequently, the cells were washed with PBS to remove any unbound dye. Fluorescence images were then acquired using an Olympus fluorescence microscope, and the intensity of the fluorescence signals was quantified. For quantitative reverse transcription-polymerase chain reaction (qRT-PCR), total RNA was extracted from tissues or cultured cells using TRIzol reagent (Biyuntian, Wuxi, China), and its concentration was determined spectrophotometrically. Complementary DNA (cDNA) was then synthesized, and quantitative PCR was performed using SYBR Green assays with gene-specific primers according to the manufacturer's protocol (Vazyme, Nanjing, China). Relative gene expression levels were normalized to the endogenous control gene *GAPDH*. For Western blotting, total proteins from clinical samples and cultured cells were harvested using RIPA lysis buffer containing a protease inhibitor cocktail. Proteins were separated by 10–12.5% SDS-PAGE and transferred to PVDF membranes, which were subsequently blocked with 8% non-fat milk for 40 min at room temperature. Primary antibodies were incubated for 10 hours at 4 °C, followed by HRP-conjugated secondary antibodies for 55 minutes at room temperature. Target protein bands were visualized using an Enhanced Chemiluminescence (ECL) detection system using X-ray films. Due to varied laboratory supplies, two types of protein molecular weight markers were used: pre-stained (visible under X-ray film) and non-stained (non-visible under X-ray film). For blots using the non-stained but colorful ladder, the PVDF membrane was cut post-transfer based on the predicted molecular weight of the target band, leaving approximately a window (15–20 kD above and below the target). This portion was marked on the X-ray film for alignment. For all conditions, the primary image was captured using X-ray film. The target band and its surrounding area were then cropped to a rectangular outline for presentation. This rectangular image was imported into Adobe Photoshop to crop the final band to the Figure's desired width. Full, uncropped rectangular blotting images, including molecular markers (or their marked alignment), are provided in Source Data.

For co-immunoprecipitation (Co-IP), total cellular lysates (0.5 mg total lysates per sample) were incubated with the primary antibody for 10 h at 4 °C to capture the protein complex. Protein A/Sepharose beads (Amersham Biosciences, Shanghai, China) were then used to precipitate the complex, which was subsequently washed, eluted, and subjected to Western blotting for interaction protein identification. The parallel "sister" gels were utilized for examining different proteins in the same lysates, when necessary.

Sprouting assay

Following treatment, hRMECs were harvested and coated onto Cytodex 3 microcarrier beads (GE Healthcare, Shanghai, China). These coated beads were subsequently embedded in 2 mg/mL fibrin gels prepared in 24-well plates by mixing 2 mg/mL fibrinogen (Calbiochem, Darmstadt, Germany) with PBS, 0.625 U/mL thrombin (Sigma-Aldrich), and 0.15 U/mL aprotinin (Sigma-Aldrich). The endothelial basal medium containing 20,000 hRMECs per well was then added. The cultures were maintained for designated time. Bright-field images were acquired using an inverted microscope (Olympus, Japan). The number of sprouts and the average length of each sprout were quantified using the Sprout Morphology plugin in Fiji (ImageJ).

Mitochondrial morphological analysis

Mitochondrial morphology was assessed using immunofluorescence staining for the mitochondrial outer membrane protein TOM20, in conjunction with transmission electron microscopy (TEM). hRMECs were fixed with 4% paraformaldehyde for 15 min, permeabilized with 0.1% Triton X-100 for 10 min, and blocked with 5% BSA for 1 h. The cells were then incubated with anti-TOM20-Alexa Fluor 488 antibody (Abcam, Shanghai, China) for 2 h and counterstained with DAPI for 5 min. Images were captured using fluorescence microscope (Olympus, Japan) to visualize mitochondrial morphology. Quantitative analysis of mitochondrial branch length, area, and network branch count was performed using the MiNA plugin in Fiji from ImageJ software. For TEM analysis, hRMECs were cultured in 10-cm dishes to achieve approximately 50-60% confluence. Cells were fixed with the electron microscopy fixative glutaraldehyde at 4 °C. The ultrastructure of the mitochondria was subsequently examined using a TEM Hitachi HT7700, yielding detailed insights into mitochondrial morphology and organization.

Metabolic analysis

Metabolic assessments were conducted using the Seahorse XF96 extracellular flux analyzer (Agilent Technologies, Santa Clara, CA) based on the attached protocols. In brief, hRMECs were seeded at 4×10^4 cells per well in 96-well plates. For the glycolysis stress test, 10 mM glucose, 1.5 μM oligomycin, and 50 mM 2-deoxyglucose (2-DG) were added to measure extracellular acidification rate (ECAR), assessing maximum glycolytic capacity and glycolytic reserve. In the mitochondrial stress test, 1.5 μM oligomycin was added for ATP production, followed by 1.5 μM FCCP to evaluate maximal respiration and a mix of antimycin A (2.5 μM) and rotenone (2.5 μM) to inhibit the electron transport chain. Key parameters included basal oxygen consumption rate (OCR), spare capacity, and proton leak, with basal OCR indicating resting respiration and spare capacity reflecting metabolic flexibility. Proton leak was determined by the OCR after oligomycin treatment.

Proteomic sequencing and functional analysis

Samples from the designated hRMECs underwent label-free proteomic sequencing at Genechem Biotechnology (Shanghai, China). For the proteomic analysis, proteins were classified as differentially expressed if at least 50% of the replicate data within the sample group showed non-null values, with a fold change exceeding 1.5 (either upregulated or downregulated) and an adjusted *P*-value below 0.05. The differentially expressed proteins and genes were then analyzed for Gene Ontology (GO) functional enrichment using the Enrichr tool.

SUMOylation sites prediction

SUMOylation sites were identified utilizing the JASSA and SUMOplot programs. Protein sequences of Gαi1/3 from six different species (Homo sapiens, Mus musculus, Rattus norvegicus, Gallus gallus, American chameleon, Xenopus laevis, and Danio rerio) were retrieved from the UniProt database (https://www.uniprot.org/) and aligned using the T-Coffee tool (https://www.ebi.ac.uk/jdispatcher/msa/tcoffee?stype=protein).

Polysome profiling and PCR analysis

hRMECs (1×10^7 cells per sample) were subjected to polysome profiling by first lysing cells on ice for 30 min in 300–500 μL of polysome profiling lysis buffer (QingZebio, Guangzhou). Cleared lysates (100 μL) were then layered onto continuous 10–45% (w/v) linear sucrose gradients, which were prepared using Polysome profiling sucrose buffer (QingZebio, Guangzhou) and an automated density gradient preparation system (Biocomp, Canada). These gradients were centrifuged in an SW41 rotor using a Beckman Optima XE-90 ultracentrifuge (Beckman Coulter, Germany) at $2.2 \times 10^5 g$ for 3 h at 4 °C. Fractions were collected with continuous absorbance monitoring at 260 nm (OD) to generate polysome profiles, and these fractions were immediately stored at −80 °C. RNA was subsequently extracted from these collected fractions, followed by qRT-PCR analysis.

Statistical analysis

Data conforming to a normal distribution were expressed as mean ± standard deviation (S.D.). No data were excluded. Sample collection was not blinded, but a blinded investigator without knowing the group

distribution performed the subsequent data analysis. To assess statistical differences between two specific groups, a two-tailed unpaired t-test was employed. For comparisons involving three or more groups, one-way analysis of variance (ANOVA) followed by Bonferroni's post hoc test was utilized. The term "biological repeats" refers to experiments conducted at different time points using independently prepared cell cultures. A *P*-value of less than 0.05 was considered statistically significant.

Reporting summary

Further information on research design is available in the Nature Portfolio Reporting Summary linked to this article.

Data availability

The scRNA-seq and RNA-seq files in Figs. 1, 2 and Fig. S2 are from publicly available sources (GSE150703, GSE175895, GSE135922, GSE94019, and GSE60436). The proteomic sequencing data have been deposited to the ProteomeXchange Consortium via the PRIDE partner repository with the dataset identifier PXD063519. Source data are provided with this paper. All data needed to evaluate the conclusions in the paper are present in the paper and the Supplementary Materials. The newly-generated materials are available in Figures and the Supplementary Files. Source data are provided with this paper.

References

1. Cao, Y., Langer, R. & Ferrara, N. Targeting angiogenesis in oncology, ophthalmology and beyond. *Nat. Rev. Drug Discov.* **22**, 476–495 (2023).
2. Selvam, S., Kumar, T. & Fruttiger, M. Retinal vasculature development in health and disease. *Prog. Retin Eye Res.* **63**, 1–19 (2018).
3. Gariano, R. F. & Gardner, T. W. Retinal angiogenesis in development and disease. *Nature* **438**, 960–966 (2005).
4. Helotera, H. & Kaarniranta, K. A Linkage between Angiogenesis and Inflammation in Neovascular Age-Related Macular Degeneration. *Cells* **11**, 3453 (2022).
5. Antonetti, D. A., Silva, P. S. & Stitt, A. W. Current understanding of the molecular and cellular pathology of diabetic retinopathy. *Nat. Rev. Endocrinol.* **17**, 195–206 (2021).
6. Dudley, A. C. & Griffioen, A. W. Pathological angiogenesis: mechanisms and therapeutic strategies. *Angiogenesis* **26**, 313–347 (2023).
7. Eelen, G., Treps, L., Li, X. & Carmeliet, P. Basic and Therapeutic Aspects of Angiogenesis Updated. *Circ. Res.* **127**, 310–329 (2020).
8. Liu, Z. L., Chen, H. H., Zheng, L. L., Sun, L. P. & Shi, L. Angiogenic signaling pathways and anti-angiogenic therapy for cancer. *Signal Transduct. Target Ther.* **8**, 198 (2023).
9. Kretschmer, M., Rudiger, D. & Zahler, S. Mechanical Aspects of Angiogenesis. *Cancers (Basel)* **13**, 4987 (2021).
10. Luo, Z., Yao, J., Wang, Z. & Xu, J. Mitochondria in endothelial cells angiogenesis and function: current understanding and future perspectives. *J. Transl. Med.* **21**, 441 (2023).
11. Caja, S. & Enriquez, J. A. Mitochondria in endothelial cells: Sensors and integrators of environmental cues. *Redox Biol.* **12**, 821–827 (2017).
12. Kluge, M. A., Fetterman, J. L. & Vita, J. A. Mitochondria and endothelial function. *Circ. Res.* **112**, 1171–1188 (2013).
13. Rensvold, J. W. et al. Defining mitochondrial protein functions through deep multiomic profiling. *Nature* **606**, 382–388 (2022).
14. Ma, Z. et al. Identification and analysis of mitochondria-related central genes in steroid-induced osteonecrosis of the femoral head, along with drug prediction. *Front Endocrinol. (Lausanne)* **15**, 1341366 (2024).
15. Chen, Z. et al. A novel prognostic signature based on four glycolysis-related genes predicts survival and clinical risk of hepatocellular carcinoma. *J. Clin. Lab Anal.* **35**, e24005 (2021).
16. Park, J. C. et al. Fine-tuning GPCR-mediated neuromodulation by biasing signaling through different G protein subunits. *Mol. Cell* **83**, 2540–2558.e2512 (2023).
17. Rysiewicz, B., Blasiak, E., Mystek, P., Dziedzicka-Wasylewska, M. & Polit, A. Beyond the G protein alpha subunit: investigating the functional impact of other components of the Galphai(3) heterotrimers. *Cell Commun. Signal* **21**, 279 (2023).
18. Xu, G. et al. Galphai1/3 mediation of Akt-mTOR activation is important for RSPO3-induced angiogenesis. *Protein Cell* **14**, 217–222 (2023).
19. Shan, H. J. et al. SCF/c-Kit-activated signaling and angiogenesis require Galphai1 and Galphai3. *Int J. Biol. Sci.* **19**, 1910–1924 (2023).
20. Li, Y. et al. Galphai1/3 mediate Netrin-1-CD146-activated signaling and angiogenesis. *Theranostics* **13**, 2319–2336 (2023).
21. Yao, J. et al. The requirement of phosphoenolpyruvate carboxykinase 1 for angiogenesis in vitro and in vivo. *Sci. Adv.* **8**, eabn6928 (2022).
22. Sun, J. et al. Galphai1 and Galphai3mediate VEGF-induced VEGFR2 endocytosis, signaling and angiogenesis. *Theranostics* **8**, 4695–4709 (2018).
23. Scott, A. & Fruttiger, M. Oxygen-induced retinopathy: a model for vascular pathology in the retina. *Eye* **24**, 416–421 (2010).
24. Campochiaro, P. A. Molecular pathogenesis of retinal and choroidal vascular diseases. *Prog. Retin Eye Res.* **49**, 67–81 (2015).
25. Reichard, A. & Asosingh, K. The role of mitochondria in angiogenesis. *Mol. Biol. Rep.* **46**, 1393–1400 (2019).
26. Marcu, R., Zheng, Y. & Hawkins, B. J. Mitochondria and angiogenesis. *Adv. Exp. Med Biol.* **982**, 371–406 (2017).
27. Wang, C. et al. FUNDC1-dependent mitochondria-associated endoplasmic reticulum membranes are involved in angiogenesis and neoangiogenesis. *Nat. Commun.* **12**, 2616 (2021).
28. Ren, R. et al. PKM2 regulates angiogenesis of VR-EPCs through modulating glycolysis, mitochondrial fission, and fusion. *J. Cell Physiol.* **235**, 6204–6217 (2020).
29. Ma, Z. R. et al. The mitochondrial protein TIMM44 is required for angiogenesis in vitro and in vivo. *Cell Death Dis.* **14**, 307 (2023).
30. Huan, M. J. et al. Identification of the central role of RNA polymerase mitochondrial for angiogenesis. *Cell Commun. Signal* **22**, 343 (2024).
31. Xiong, Q. W. et al. The requirement of the mitochondrial protein NDUFS8 for angiogenesis. *Cell Death Dis.* **15**, 253 (2024).
32. Wu, W. et al. PI3Kdelta as a Novel Therapeutic Target in Pathological Angiogenesis. *Diabetes* **69**, 736–748 (2020).
33. Sharma, D. et al. IL-33 enhances Jagged1-mediated NOTCH1 intracellular domain (NICD) deubiquitination and pathological angiogenesis in proliferative retinopathy. *Commun. Biol.* **5**, 479 (2022).
34. Li, J. et al. Endothelial TWIST1 promotes pathological ocular angiogenesis. *Invest Ophthalmol. Vis. Sci.* **55**, 8267–8277 (2014).
35. Iizuka, N. et al. Anti-angiogenic effects of valproic acid in a mouse model of oxygen-induced retinopathy. *J. Pharm. Sci.* **138**, 203–208 (2018).
36. Yetkin-Arik, B. et al. The role of glycolysis and mitochondrial respiration in the formation and functioning of endothelial tip cells during angiogenesis. *Sci. Rep.* **9**, 12608 (2019).
37. Diebold, L. P. et al. Mitochondrial complex III is necessary for endothelial cell proliferation during angiogenesis. *Nat. Metab.* **1**, 158–171 (2019).
38. Lugus, J. J., Ngoh, G. A., Bachschmid, M. M. & Walsh, K. Mitofusins are required for angiogenic function and modulate different signaling pathways in cultured endothelial cells. *J. Mol. Cell. Cardiol.* **51**, 885–893 (2011).
39. Li, J. et al. Cbx4 governs HIF-1alpha to potentiate angiogenesis of hepatocellular carcinoma by its SUMO E3 ligase activity. *Cancer Cell* **25**, 118–131 (2014).
40. Zhou, H. J. et al. SUMOylation of VEGFR2 regulates its intracellular trafficking and pathological angiogenesis. *Nat. Commun.* **9**, 3303 (2018).

41. Wang, Y. et al. Neuronal-driven glioma growth requires Galphai1 and Galphai3. *Theranostics* **11**, 8535–8549 (2021).
42. Marshall, J. et al. Antidepression action of BDNF requires and is mimicked by Galphai1/3 expression in the hippocampus. *Proc. Natl Acad. Sci. USA* **115**, E3549–E3558 (2018).
43. Liu, Y. Y. et al. microRNA-200a downregulation in human glioma leads to Galphai1 over-expression, Akt activation, and cell proliferation. *Oncogene* **37**, 2890–2902 (2018).
44. Zhang, Y. M. et al. Requirement of Galphai1/3-Gab1 signaling complex for keratinocyte growth factor-induced PI3K-AKT-mTORC1 activation. *J. Invest Dermatol* **135**, 181–191 (2015).
45. Cao, C. et al. Galpha(i1) and Galpha(i3) are required for epidermal growth factor-mediated activation of the Akt-mTORC1 pathway. *Sci. Signal* **2**, ra17 (2009).
46. Bai, J. Y. et al. Requirement of Galphai1 and Galphai3 in interleukin-4-induced signaling, macrophage M2 polarization and allergic asthma response. *Theranostics* **11**, 4894–4909 (2021).
47. Li, X. et al. Galphai1 and Galphai3 regulate macrophage polarization by forming a complex containing CD14 and Gab1. *Proc. Natl Acad. Sci. USA* **112**, 4731–4736 (2015).
48. Voigt, A. P. et al. Single-cell transcriptomics of the human retinal pigment epithelium and choroid in health and macular degeneration. *Proc. Natl Acad. Sci. USA* **116**, 24100–24107 (2019).
49. Weinstein, N., Mendoza, L., Gitler, I. & Klapp, J. A network model to explore the effect of the micro-environment on endothelial cell behavior during angiogenesis. *Front Physiol.* **8**, 960 (2017).
50. Blancas, A. A., Wong, L. E., Glaser, D. E. & McCloskey, K. E. Specialized tip/stalk-like and phalanx-like endothelial cells from embryonic stem cells. *Stem Cells Dev.* **22**, 1398–1407 (2013).

Acknowledgements

We thank Dr. Zai-xiang Tang from Soochow University for validating the utilization of suitable statistical tests in this study. This work was supported by generous funding from the National Natural Science Foundation of China (82571750, 82371473, 82171461 and 81922025 to C.C., 82070983 to Q.J., 82571243 and 82271107 to J.Y. and 82571232 and 82171080 to K.R.L.), Jiangsu Province Social Development Project (BE2023702, to C.C.), a Project Funded by the Priority Academic Program Development of Jiangsu Higher Education Institutions, the Natural Science Foundation of Jiangsu Province (BK20221186 to J.Y.), Jiangsu Provincial Health Commission Medical Research Key Project (K2023060 to J.Y., BK20240122 to K.R.L.) and Postgraduate Research and Practice Innovation Program of Jiangsu Province (JX10414318 to J.Y., JX10414322 to K.R.L.). The funders had no role in the study design, data collection and analysis, decision to publish, or preparation of the manuscript.

Author contributions

W.B., D.P.Y., G.C., Y.L., Q.J., K.R.L., J.Y., and C.C. proposed and designed the research. W.B., D.P.Y., G.C., Y.L., K.R.L., J.Y., and C.C. performed the experiments, analyzed the data, and organized the figures. Q.J., K.R.L., J.Y., and C.C. supervised the research. K.R.L., J.Y., and C.C. are responsible for funding acquisition, project administration, and revision. W.B., D.P.Y., G.C., Y.L., K.R.L., J.Y., and C.C. wrote the manuscript, and all authors contributed to the discussion of the experiments and the final manuscript.

Competing interests

The authors declare no competing interests.

Additional information

Supplementary information The online version contains supplementary material available at https://doi.org/10.1038/s41467-025-66212-x.

Correspondence and requests for materials should be addressed to Ke-ran Li, Jin Yao or Cong Cao.

Peer review information *Nature Communications* thanks David Li, and the other, anonymous, reviewer(s) for their contribution to the peer review of this work. A peer review file is available.